A symmetry analysis on Chirality Induced Spin Selectivity in two-terminal transport

by

J.W.J. (Jochem) van de Kamp

to obtain the degrees of Bsc. Applied Mathematics and Bsc. Applied Physics
at the Delft University of Technology,
to be defended publicly on Wednesday November 12, 2025 at 14:00 PM.

Student number:	5171679	
Project duration:	March 14, 2024 – November 5, 2025	
Thesis committee:	Prof. Dr. J. M. Thijssen,	TU Delft, supervisor AP
	Dr. J. L. A. Dubbeldam,	TU Delft, supervisor AM
	Dr. M. T. Wimmer,	TU Delft, member AP
	Dr. Ir. W. G. M. Groenevelt	TU Delft, member AM

An electronic version of this thesis is available at `http://repository.tudelft.nl/`.
The Python script of the model is available at
`https://github.com/Jochemvandekamp/CISS_symmetries`.

TU Delft

Abstract

Chirality Induced Spin Selectivity is the phenomenon where the chirality of certain molecules favours the transmission of electrons based on their spin. Among many examples, this long-studied phenomenon appears in two terminal transport experiments,where different magnetisations of the leads can give different current-voltage characteristics. In previous research by Rikken [20], the chiral geometry of the device was determined as a necessary condition for antisymmetric IV curves.
In this thesis, we implemented a Büttiker probe (BP) in a 6-helicene model based on the previous work of Geyer [9]. The probe mimics the decoherence in a two-terminal CISS experiment. Moreover, this enables us to magnetise both leads independently. By altering the magnetisation of the leads and the orientation of the Büttiker probe, we were able to analyse many possible experimental setups. This enabled us to express the current difference in terms of bias voltage, magnetisation and BP orientation, where the latter was the research objective.
Isotropic Büttiker probes lead to a CISS effect, which is absent in a coherent electron transport model. Further research is needed to determine the exact nature of the numerical errors in our isotropic BP experiments. The results of anisotopic BPs can be explained assuming that the current difference is linear in the anisotropy of the BP. Further research is needed to strengthen this conjecture. These results are supported for lead magnetisation along an axis, perpendicular on the helical axis of the molecule, as well as magnetisation along this helical axis.

Contents

[1] We assume a basic understanding of the general use of Greens functions. It was not feasible to include either long derivations in the specific context of quantum mechanics, nor to include proof of existence for the Greens functions and general applicability. For a more fundamental (basic) study on Green's functions, see [8].

1

Introduction

Chirality Induced Spin Selectivity is a widely measured phenomenon where the transmission of electrons depends on the handedness (chirality) of the molecule. When electrons pass through a chiral molecule, one spin orientation is favoured over the other. This means that the molecular structure itself controls the transmission of electrons based on their spin. Since the 1990s, physicist have found this effect in a wide range of materials and experimental setups [19],[24],[11], and this kept their interest for almost three decades. Many models were built to explain the driving forces behind this effect, but all failed to provide a theory that can explain CISS quantitively. A better understanding of the CISS effect could prove to be a concrete basis for the development of spintronics: a technology where information is stored in the spin of the electrons.
In this thesis we perform a thorough analysis of the Chirality Induced Spin Selectivity in a two-terminal system. In two-terminal measurements on chiral molecules, one of the leads is magnetized and the current is measured for opposite magnetisations. Results are computed with a model based on previous work by Geyer and Visscher. We introduced a Büttiker probe to according to the work by Bedkihal. The Büttiker probe introduces a disruptive, symmetry breaking force, which allows us to measure a spin dependent transmission. Based on the results, we come to a conclusion on the symmetrical properties of the current difference and current polarisation.
Chapter 2 provides an summary of the previous work, along with a more detailed description of the CISS effect in two terminal transport. We also take a look at the symmetries involved in our experiments and we define the research objective for this thesis. In chapter 3, we discuss the theoretical background relevant to our research. This involves Onsager's reciprocal theorem, which Chapter 4 concerns the theory behind the interaction of the molecule and the surroundings. On the one hand, we have the complexity of the leads, where the Non-equilibrium Green's function formalism will provide a way involve the lead mathematically as two semi-infinite electron bath's. On the other hand, we explain the mathematical framework for the Büttiker probe, which will provide essential decoherence to our electron transport. The mentioned model will be explained in detail in chapter 5, and chapter 6 will show and analyse the results. Finally, chapter 7 provides a conclusion of the results in chapter 6, and proposes avenues for future research.

2

Chirality Induced Spin Selectivity

2.1. Chirality

Chirality is a characteristic of any spatial object. It is used to describe two different but similar objects, which are the mirror image of each other but cannot be transformed into each other by rotation and translation. A simple example is your hands, as the ancient Greek word for hand, $\chi\epsilon\iota\rho$, gave the name to such objects. In chemistry, one of such two mirror images is called an enantiomer, where prefixes like l, r, or s, and d are used to distinguish one from the other. For this thesis, a helical object, helicene, is used. Those two enantiomers differ in their curvature, where we have a clockwise- and anticlockwise-oriented molecule. See Figure 2.1 for a schematic model of the two possible (6)-helicene enantiomers.

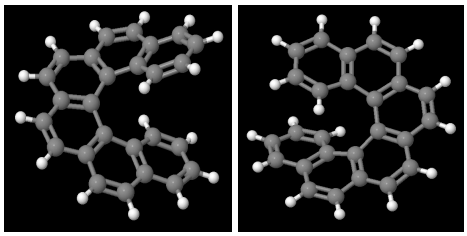

Figure 2.1: The clockwise and anticlockwise enantiomer of (6)-helicene. The molecule is called chiral as one cannot find the clockwise orientation by simply rotating the anticlockwise molecule, but a mirror operation is needed.

2.2. Chirality induced spin selectivity

For chiral molecules, Ray et al. discovered a new phenomenon in 1999 [19]. An experiment was conducted in which a polarised light beam induced an electron beam by the photoelectric effect.[1] An analysis of the electron beam yielded a remarkable result: the transmissions for spin-up and spin-down electrons were found to be different. The experiment was repeated with different kinds of chiral molecules and other metallic layers with varying asymmetry. Generally, researchers were able to find a significant difference in transmission.

Interest in further research was sparked by possible applications in spintronics. Where the current binary computers built their logic only on the presence of electrons, i.e. a 0 for no electrons, and a 1 for electrons, it might be possible to extend the classical computers to triplet logic gates. In this case, the logic information represented by a current could be split in a (mostly) spin-up current and a (mostly) spin-down current, enabling a logic gate to generate three potential outputs. This could all be done by something as small as a single molecule, which is significant in an age where everyday chips contain billions of logic gates. Moreover, a deeper understanding of the forces behind the transmission difference would give us a better understanding of the symmetries of life. Most enzymes we can produce

[1] **The photoelectric effect:** When light with enough energy hits an electron in orbit around a nucleus, the electron can absorb this photon and the energy will enable the electron to leave the orbit. On a larger scale, a material will seem to emit an electron beam as a result of the incoming light beam. The discovery of this effect received Einstein his Nobel Prize in Physics in 1921.

ourselves are oriented to the left, where DNA is oriented to the right. This asymmetry, called homochirality, could tell us more about the conditions for early life and give us a better understanding about the most fundamental forces that shaped everyday life [1].

2.2.1. Symmetry and chirality

Symmetry is defined by symmetry operations. If an action is applied and the object appears to be unaffected, then we call the object symmetric with respect to the associated symmetry operation. In this thesis, we involve two types of symmetry, molecular symmetry operations and fundamental symmetries of times and space [25].

Molecular symmetry operations

Molecular symmetry operations are spatial operations: movement of the molecule according to the rules imposed by the symmetry operation would not result in any apparent change. The scientific consensus describes five different types of molecular symmetry operations. These are shown in table 2.1, adapted from reference [25].

Table 2.1: Molecular symmetry operations

	Symmetry operation	Symmetry element	Definition
$\hat{E}$	identity	the object itself	doing nothing
$\hat{C}_n$	n-fold proper rotation	an axis of symmetry	rotating the object by $2\pi/n$ around the axis[a]
$\hat{\sigma}$	reflection	a mirror plane	reflecting the object with respect to the plane[b]
$\hat{i}$	inversion	a center of symmetry	inverting the object with respect to the center
$\hat{S}_n$	n-fold improper rotation	a rotatory reflection axis	an n-fold proper rotation followed by a reflection[c]

[a] For an object with multiple rotational axes, the one with largest value n is called the *principal axis* of symmetry.
[b] When the mirror plane contains the principal axis of symmetry, it is *vertical*, and the symmetry operation is denoted $\hat{\sigma}_v$. A *horizontal* plane is perpendicular to the principal axis and is denoted $\hat{\sigma}_h$.
[c] The reflection mirror plane is perpendicular to the rotational axis.

Table 2.1 introduces the *symmetry element*. This is element on which the operator works. For example, rotation needs a pivotal point. An object symmetric under rotation must therefore contain a point around which it can rotate without a visible change in rotation.
We call the molecule chiral, of it is not symmetric under any improper rotation $\hat{S}_n$. As we have that $\hat{S}_1 \equiv \hat{\sigma}$ and $\hat{S}_2 \equiv \hat{i}$, a chiral molecule does not have reflection or inversion symmetries, as seen in section 2.1..

Time-reversal symmetry

So far, we only took a look at spatial symmetries, and found a different definition for a chiral molecule. However, in all CISS experiments, we describe a phenomenon in transport, which is a time dependent process. Therefore we introduce the symmetry operation of *time-reversal* $(\hat{T})$. We use this operation to describe the reversibility of all motion. When a system is appears unaffected under time reversal, it is called time-reversal symmetric or invariant under time-reversal. In theoretical physics, this is one of the three fundamental symmetry operations, together with charge conjugation $\hat{C}$ and parity $\hat{P}$[2].
Theoretically, we commonly describe these operators as either even or odd. Parity-odd arguments as vectors change sign when the operator is inflected[3]. These vectors are called polar vectors. Parity even vectors are called axial vectors, as for example, angular momentum retains sign. Thus a cross product of two odd vectors will create a $\hat{P}$-even vector. Similarly, we can sort physical quantities as time-odd or time-even function. Time-odd function always involve motion. For example, both magnetic field $\underline{B}$ as magnetization $\underline{M}$ are defined by the *movement* of charge, and therefore time-odd. This can be seen more intuitively, when we try to reverse time be rewinding our measurement. The charges will move in opposite direction, and thus the $\underline{B}$-field that they generate, will be oriented in opposite direction. On the other hand, the electric field $\underline{E}$ is $\hat{T}$-even, as it is defined by stationary displacement of electric charges.
After extensive study of these symmetries, Barron introduced the concept of true chirality, based on the previous mentioned, $\hat{P}$ and $\hat{T}$ symmetries [2]. True chirality can be best shown in a helix shaped molecule, like the one of our interest. (6)-helicene is true chiral, as we need a space inversion to change

[2] This is also described as space-inversion: $\hat{x}, \hat{y}, \hat{z} \rightarrow -\hat{x}, -\hat{y}, -\hat{z}$
[3] This is analogue to odd functions, as $f(-x) = -f(x)$

its handedness. However, we can force electrons through the same path by strategically placing both collinear $\underline{E}$ and $\underline{B}$ fields. In this case, time reversal would change the handedness (the observed chirality) as well, as $\underline{B}$ fields are time-odd. Failing to note the implication of true chirality has lead to numerous failed attempts to separate enantiomers. Any hypothesis on symmetry of CISS effects must therefore a carefully drawn.

2.2.2. CISS in two terminal transport

The (6)-helicene model, as it will be described in Chapter 5, is an example of the CISS effect on two-terminal transport. In this case, we take the chiral helicene and place it between two leads. One of the leads in the setup is magnetised. To generate a current, we apply a voltage difference over the two leads, called the bias voltage. The generated current is commonly referred to as the magnetocurrent. We measure the currents as a function of the voltage for opposite directions of the magnetisation to determine the polarisation of the current:

$$P_{current} = \frac{I(m) - I(-m)}{I(m) + I(-m)} \tag{2.1}$$

This expression quantifies the CISS effect through the magnetisation including the effect of the potential V. It is commonly odd in this bias voltage.

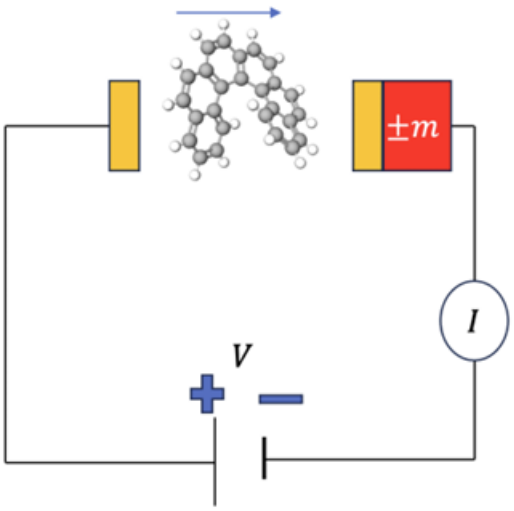

Figure 2.2: Schematic overview of the (6)-helicene experiment. The bias voltage V generates a magnetocurrent I through the chiral molecule. The transmission bias is measured for magnetisation in both direction with magnitude m. Adapted from [14].

Qualitative theories have tried to formulate some explanation to the mysteries surrounding the CISS effect, and even reach some consensus about its nature. For example, two terminal transport is described best on mesoscopic scale. When an electron moves through the chiral molecule, we measure the relativistic interaction between the electron spin and its angular momentum around the atoms in the helicene molecule. Consequently, only electrons with spin up show transmission through the molecule. However, when these electrons reach the magnet at the second lead, Pauli's principle does not allow for transmission of spin up electrons, and this interaction reverses the direction of momentum of the electron. The electron is now travelling backwards, but encounters the same chirality of the helicene molecule, which does not allow for transmission. This keeps the electron captured between the chiral molecule and the magnet, was it not for the spin-orbit coupling. This coupling allows the electron to flip its spin and lays the foundation for the chiral induced spin selectivity.

2.2.3. Spin-Polarisation

The previously described transmission is denoted by $T(\epsilon)$, with ϵ the energy of the electron. One can determine the current through the system by integration over all possible energies.[4] Relevant differences of the transmission in our experiment stem from three sources:

1. The energy of the electrons as a result from the electric bias. At low energies, the energy is always close to the Fermi energy. Thus transmission is a function of energy ϵ.
2. The terminals the electron travels to and from: the involved terminals are described in the subscript of T.[5]
3. The spinstate related to each of the terminals. As described above, the transmission is not equal for spin up and spin down electrons. The associated spinstates in the arrow notation are given in the superscript.

We can define the spin polarisation as a function of the transmission from the left (L) to the right (R) lead as follows:

$$P(\epsilon) = \frac{T_{LR}^{\uparrow\uparrow}(\epsilon) + T_{LR}^{\downarrow\uparrow} - T_{LR}^{\uparrow\downarrow} - T_{LR}^{\downarrow\downarrow}}{T_{LR}^{\uparrow\uparrow} + T_{LR}^{\downarrow\uparrow} + T_{LR}^{\uparrow\downarrow} + T_{LR}^{\downarrow\downarrow}} \tag{2.2}$$

where T is an energy dependent transmission probability. The superscript denotes the spin polarisation at the left and right lead respectively. The transmission functions $T_{LR}^{\downarrow\uparrow}$ and $T_{LR}^{\uparrow\downarrow}$ are of particular interest as it is related to the CISS effect specifically.
However, it is a function of energy ϵ, and the current polarisation in 2.1 shows a dependence on the magnetisation of the leads. This interacts with the electron spin, and it forces the electron to align with the direction of the magnetisation. To account for this interaction, we use projection matrices that depend on the *spin* polarisation p. The construct of these projection matrices can be found in appendix A.5.

2.2.4. Research objective

As we mentioned previously in this chapter, the current polarisation is commonly odd in V. However, the effect of the magnetisation has not been studied yet. In reference [20], Rikken summarizes the consensus on CISS magneto-resistance (CISS-MR). Results for the IV-graph are antisymmetric over the voltage and symmetric in the handedness. Symmetry in handedness means that the spin-up transmission in the L enantiomer is identical to the spin-down transmission in the D enantiomer, although exceptions have been reported. The research objective of this thesis is about the rotation symmetry in the magnetisation. Rikken claims that antisymmetric results for an IV-curve are impossible due to $\hat{P}$-odd behaviour of the magnetisation. Any reported antisymmetric IV-curve must be generated by an asymmetric setup.
In this thesis, we built on the model of Geyer [9], where we split the magnetisation over both leads. Therefore it is now virtually possible to create a symmetric setup. Here, we read out the magnetocurrent for multiple spin polarisations, both along the axial vector of the molecule, as the axis perpendicular to it. The transport of electrons is essentially coherent in this model. However, impurities like phonons will always lead to decoherence in the experimental setup. To mimic this decoherence, we will use the proven method of a Büttiker probe. This is a terminal similar to the leads, but its chemical potential is set in such way, that this terminal shall not draw any current. We can orient the Büttiker probe in different directions, either along or perpendicular to the axis of magnetisation. Eventually, we will determine the effect of different magnetisations and orientations of the Büttiker probe with the goal of establishing the effect of relative magnetisation and decoherence.

[4] The possibility of energies is limited by the bias voltage, so integrals run from $-V$ to V.
[5] The transmission is symmetric in the direction. An intuitive explanation can be found in section 4.4

3

Equilibrium analysis: Onsager's reciprocal theorem

The Onsager reciprocal relations are named after Lars Onsager. In 1931, he made a significant contribution to the mathematical framework around thermodynamics on a microscopic level. For his derivations, he won the Nobel Prize. Firstly, we describe the tricky nature of thermodynamics to show the challenge ahead. We focus on the thermodynamics in a thermodynamic equilibrium. Then we will we take a deep dive in the mathematical framework created by Onsager. Finally, we shall see how this all connects to our challenge with the CISS-effect and how his theorem applies to CISS-experiments.

3.1. Introduction

The field of statistical mechanics is quite a new one, but before Onsager came to his contribution, the basis of statistical mechanics was firmly placed on a set of **statistical ensembles** introduced by Gibbs in 1902 [10]. Such an ensemble contains all possible copies which describe the same system. See, for example [21] for a deeper dive into the fundamental theorem in statistical mechanics.
The possible ensembles is almost limitless. One particular interesting ensemble that was already described by Gibbs is the microcanonical ensemble. It contains all the possible states of a system with a single, fixed energy, volume and particle number. In this case, we assume that all microstates are equally probable. In quantum mechanics, this ensemble is described by a Hamiltonian.
To make the link to entropy, we take for example an isolated, gaseous system. If a gas is released into air, then this new gas will spread through diffusion. This is a passive process that does not require any form of force, and therefore work. In the beginning, there is a lot of potential for diffusion, or more generally speaking, thermodynamic potential. At first, all the molecules are packed together at the point of release. The options to model this situation are limited, we need to put all the molecules together on the micro level, to create the related macro level, where all the as is still densely packed. The count of all the possible microscopic arrangements that describe the same macroscopic state is called the multiplicity Ω. This quantity is directly related to the entropy of the system. As the gas diffuses, the new gas molecules are distributed quite evenly in the system, which allows for more microstates, thus a greater multiplicity, and therefore more entropy. We conclude that diffusion is a passive process, work requires energy, and that was fixed in the system. Statistical mechanics thus allows for the new gas to be densely packed together after any amount of time. However, the odds of that happening are infinitesimal. In practice, the system will always go to a macrostate with the most microstates representing the macrostate. In our case, this is the macrostate where the new gas is spread evenly through our system. When the gas is still densely packed, the number of representing microstates is limited, but we know that the gas has a lot of potential to diffuse. This thermodynamic potential is called entropy. The relation between entropy and multiplicity is given by:

$$S = k_B \ln \Omega \tag{3.1}$$

where k_B is Boltzmann's constant. After a long time, the introduced gas is spread evenly within our system and the macrostate shall not change over time. The system is now in equilibrium as all potential to diffuse is used. Thus, the entropy reached a maximum.

3.2. Onsager's theorem

Onsager started with an arbitrary, isolated system in thermodynamic equilibrium. We express the entropy S in terms of densities of extensive parameters[1]. These densities are denoted as x_i and include, but are not limited to $\mathcal{E}/V, N/V$, where V is the fixed volume of the system.

$$S_{eq} = S(\tilde{x}_i, ..., \tilde{x}_N) \tag{3.2}$$

Now, let us consider a system close to, but not entirely within thermodynamic equilibrium. We express the entropy of such a system in terms of x_i resulting in $S(x_i, ..., x_N)$. Using the assumption that the new state is close to equilibrium, we perform a second order Taylor expansion of the entropy across all extensive parameters:

$$S(\underline{x}) = S(\underline{\tilde{x}}) + \frac{1}{2}\sum_{ij}\frac{\partial^2 S}{\partial x_i \partial x_j}(x_i - \tilde{x}_i)(x_j - \tilde{x}_j) \tag{3.3}$$

We notice that x is close to equilibrium in a mathematical way: the first differential term is not significantly unequal to zero, the first differential term in any maximum. A limitation to the second order must be justified as well.

The associated probability for any particular state $\underline{x}$ equals

$$P(\underline{x}) = \frac{e^{S(\underline{x})/k_B}}{\Omega} \text{ where } \Omega = \int e^{S(\underline{x})/k_B} dx \tag{3.4}$$

We substitute approximation 3.3 into equation 3.4. We define $\gamma_{ij} = -\frac{1}{k_B}\frac{\partial^2 S}{\partial x_i \partial x_j}$ and for the fluctuations we introduce $a_i = x_i - \tilde{x}_i$.

$$P(\underline{x}) = \frac{e^{S(\underline{x})/k_B}}{\Omega} = \frac{1}{\Omega}e^{S(\underline{\tilde{x}})} \cdot \frac{1}{\Omega}e^{-\sum_{ij}\frac{\gamma_{ij}}{2}a_i a_j} = P(a_1, a_2, .., a_N) = \frac{1}{\Omega}e^{S/k_B} \tag{3.5}$$

We continue our derivation with the goal to obtain a relation between P and S:

$$\frac{\partial P}{\partial a_k} = \frac{\partial}{\partial a_k}\left(\frac{1}{\Omega}e^{S(\underline{\tilde{x}})} \cdot e^{-\sum_{ij}\frac{\gamma_{ij}}{2}a_i a_j}\right) = -\frac{2}{\Omega}e^{S(\underline{\tilde{x}})}\sum_{ij}\frac{\gamma_{ij}}{2}a_j e^{-\sum_{ij}\frac{\gamma_{ij}}{2}a_i a_j} = -P\sum_{ij}\gamma_{ij}a_j$$

$$\frac{\partial S}{\partial a_k} = \frac{\partial}{\partial a_k}\left(S(\underline{\tilde{x}}) + \frac{1}{2}\sum_{ij}\frac{\partial^2 S}{\partial x_i \partial x_j}a_i a_j\right) = \sum_{ij}\frac{\partial^2 S}{\partial x_i \partial x_j}a_j = -k_B\sum_{ij}\gamma_{ij}a_j$$

The results of above reveal the following relation:

$$\frac{1}{P}\frac{\partial P}{\partial a_k} = \frac{1}{k_B}\frac{\partial S}{\partial a_k} \tag{3.6}$$

We use the expectation value of a_i and partial derivative of the entropy with respect to a_i to find the following expression, where we used the result of 3.6:

$$\langle a_i, \frac{\partial S}{\partial a_i}\rangle = \int a_i \frac{\partial S}{\partial a_i} P d^N a = \int a_i \frac{k_B}{P}\frac{\partial P}{\partial a_i} P d^N a = \int a_i k_B \frac{\partial P}{\partial a_i} d^N a \tag{3.7}$$

[1] extensive parameters: parameters that scale with the size of a system, such as the number of particles, the energy or the volume

We apply integration by parts to reveal:

$$k_B \int a_i \frac{\partial P}{\partial a_i} d^N a = k_B([P * a_i]_{-\infty}^{\infty} - \int P \frac{d(a_i)}{da_i} d^N a) = k_B(0-1) \tag{3.8}$$

Similarly, if $i \neq j$, we find:

$$k_B \int a_i \frac{\partial P}{\partial a_j} d^N a = k_B([P * a_i]_{-\infty}^{\infty} - \int P \frac{d(a_i)}{da_j} d^N a) = -k_B \int P \cdot 0 d^N a = 0 \tag{3.9}$$

Summerizing, we find for $\langle a_i, \frac{\partial S}{\partial a_j} \rangle$

- if $i = j$ then,
$$\langle a_i, \frac{\partial S}{\partial a_i} \rangle = k_B$$
- if $i \neq j$,
$$\langle a_i, \frac{\partial S}{\partial a_j} \rangle = 0$$

We can summarize these results in the following expression

$$-\sum_k \gamma_{ik} \langle a_k a_j \rangle = k_B \delta_{ij} = \langle \frac{\partial S}{\partial a_i} a_j \rangle \tag{3.10}$$

3.2.1. Symmetries of Onsager's reciprocal relations

We have taken a first glimpse at the symmetries in Onsager's reciprocal relations. So far, the assumptions we made still hold in a variety of systems. From this point onwards, we apply the more specific assumptions created by a system in thermodynamic equilibrium. For instance, we will assume that a system *close* to thermodynamic equilibrium has a linear response to any driving force in all of its variables in regard to the equilibrium position.

The change of entropy is therefore given by:[2]

$$\frac{dS}{dt} = \sum_i \dot{a_i} \frac{\partial S}{\partial a_i} \equiv \sum_i \dot{a_i} \chi_i \tag{3.11}$$

We see that $\chi_j = \frac{\partial S}{\partial a_j}$ is a driving force for the change of in a_i. We introduce the **linear response Ansatz**:

$$\dot{a_i} = \sum_j L_{ij} \frac{\partial S}{\partial a_j} = \sum_j L_{ij} \chi_j \tag{3.12}$$

Now, we calculate the expectation value $\langle a_i(t+\tau) a_j(t) \rangle$ for a small time difference τ. In our CISS experiment, the experimental environment includes magnetic fields and forces. The fields involved do have a direction, and must be treaten with care. We apply *time reversibility*, which will change the direction of our fields. Moving electrons create magnetic field. When we reverse the flow of time, the electron move in the opposite direction, thus this operation will invert the direction of our fields as well. Most experiments have a magnetisation of the lead, which makes $\underline{B}$ abundant. In this thesis, it is included for completeness. Firstly, extend the expectation value that includes the time difference.

$$\langle a_i(t+\tau) a_j(t) \rangle_{\underline{B},\underline{M}} = \langle a_i(t) a_j(t) \rangle_{\underline{B},\underline{M}} + \tau \langle \dot{a_i}(t) a_j(t) \rangle_{\underline{B},\underline{M}} =$$

$$\langle a_i(t) a_j(t) \rangle_{\underline{B},\underline{M}} + \tau \Sigma_m L_{im} \langle \frac{\partial S}{\partial a_m} a_j(t) \rangle_{\underline{B},\underline{M}}$$

[2] a dot above any variable is a common denotation used for the time derivative in physics

We implement the findings from 3.12 and 3.10 respectively:

$$\langle a_i(t)a_j(t)\rangle_{\underline{B},\underline{M}} + \tau\Sigma_m L_{im}\langle\frac{\partial S}{\partial a_m}a_j(t)\rangle_{\underline{B},\underline{M}} = \langle a_i(t)a_j(t)\rangle_{\underline{B},\underline{M}} + \tau\Sigma_m L_{im}\langle\chi_m a_j\rangle =$$

$$\langle a_i(t)a_j(t)\rangle_{\underline{B},\underline{M}} + \tau L_{ij}k_B \tag{3.13}$$

We extract a result for the linear response matrix through a time shift. Altough the expectation value as an operator is commutative, we do not expect this behaviour from magnetic forces. Therefore exchanging the position of two terms, leads to the change in sign of the fields. Recall that our expectation value operator is time independent, as the system is in equilibrium. We apply a time translation to find the a symmetry relation for L:

$$L_{ij}(\underline{B},\underline{M}) = \frac{1}{\tau k_B}\left(\langle a_i(t+\tau)a_j(t)\rangle_{\underline{B},\underline{M}} - \langle a_i(t)a_j(t)\rangle_{\underline{B},\underline{M}}\right) = \frac{1}{\tau k_B}\left(\langle a_j(t-\tau)a_i(t)\rangle_{\underline{B},\underline{M}} - \langle a_j(t)a_i(t)\rangle_{\underline{B},\underline{M}}\right) =$$

$$\frac{1}{\tau k_B}\left(\langle a_j(t+\tau)a_i(t)\rangle_{\underline{-B},\underline{-M}} - \langle a_j(t)a_i(t)\rangle_{\underline{-B},\underline{-M}}\right) = L_{ji}(-\underline{B},-\underline{M}) \tag{3.14}$$

This is the expected result, also known as the microscopic reversibility.

3.2.2. Onsager reciprocity and quantum coherent transport.

The Onsager reciprocity is robust as we made an analysis in non-specified extensive parameters. However, previous work [17] shows that this reciprocity breaks down quickly outside both symmetrical and linear regimes. This might be concerning, as we apply a significant bias voltage over the molecule, even so with a symmetricly applied potential division. Moreover, Onsager's statistical analysis on atomic scale must be carefully applied on mesoscopic systems. Impurities in the conductor and influence from boundary conditions break symmetry and might imply that the relations do not hold. Besides that, in a real experimental setup, the reversal of voltage (V $\rightarrow$ -V) is not generally equivalent to physically interchanging the leads attached to the probes. As shown by Büttiker [6], the symmetries in a multiterminal setup are not trivial, especially if some of the terminals act as a probe.

Implementing Onsager's reciprocal theorem on the resistance R implies that, an inversion of both current and potential would require a reversal of the magnetic field. So

$$R_{12,34}(H,M) = R_{34,12}(-H,-M) \tag{3.15}$$

However, as described by both Büttiker in ref [5] and Rikken in ref [20], we need the certainty of a symmetric system, as well as the requirement of a symmetric measurement. One must consider that on mesoscopic scale[3], small disordered conductors could break symmetry. These effects rise from the quantummechanical nature of electron transport. If the wave-like nature of the carriers plays a role, the relation between the current and the electric field cannot be local. Benoit et al. [4] derived a resistance formula for quantum coherent transport, which obeys the reciprocity relations. Hence, two-terminal transport contains a decoherence nature that is vital for the explanation of the CISS effect. The decoherence is further explained in section 4.5. The reciprocity symmetry of the S-matrix implies that:

$$R_{ii}(M) = R_{ii}(-M), \qquad T_{ij}(M) = T_{ji}(-M) \tag{3.16}$$

So an inversion of the current must be accompanied by an inversion of the magnetisation.

[3]The basic principles of electron transport on mesoscopic scale is described in appendix A.3

4

Non-equilibrium Green's function formalism

4.1. Introduction

The CISS effect is typically seen on molecular level. This makes the inclusion of quantum mechanics inevitable. The first significant landmark was the Schrödinger equation. Nowadays the starting point of many courses on QM, and the symbol of quantum mechanics on Wikipedia, the Schrödinger equation is easily skipped over by an experienced physicist. But at the heart of it, one finds the Hamiltonian operator. The Hamiltonian is an important bridge between classical and quantum mechanics. In both field of physics, the Hamiltonian expresses the energy in the (mechanical) system. However, as we recall a typical experimental setup, the challenge to find an Hamiltonian is evident. How do you describe the energy of a semi-infinite electron bath? We introduce the 'non-equilibrium Green's function formalism' (NEGF) to tackle this challenge.

4.2. The importance of Greens functions.[1]

The Green's function is named after the mathematician George Green, who made significant efforts on the mathematical description of electrical systems and devices in the 1820s. The Green's function describes the response of an inhomogeneous linear differential operator to an impulse. The Green's function is defined as:

$$LG(x,s) = \delta(x-s) \tag{4.1}$$

where $L(x)$ is the linear (differential) operator acting on G, the Green's function in one dimension x. This combination equals a function δ, which is the unit impulse function, better known to physicists as the Dirac delta function.[2] This is a function depending on the difference $x-s$, where s is the location of the point source.
The Hamiltonian is a linear operator, which we substitute for L in equation 4.1. On the right hand side, the appropriate unit impulse function is used. Eventually, we use the Greens functions to formulate the density of states in our system.

4.3. Two terminal electron transport: the density matrix

In optics, polarization of light describes the phase relation within a beam. Similarly the quantumwave of an electron has a phase, and for quantum interference to occur, those beams must be in phase. The

[1] We assume a basic understanding of the general use of Greens functions. It was not feasible to include either long derivations in the specific context of quantum mechanics, nor to include proof of existence for the Greens functions and general applicability. For a more fundamental (basic) study on Green's functions, see [8].

[2] About the continuation error: Dirac got his fame more than a century after the work done by Green. The (quantum wave) functional analysis is of the hand of Dirac, formalized by Schwartz in 1951. However, Green can be fully credited as the creator of the formalism. The only loose end he left was a mathematical formulation of the point source. However, Green had a great intuition and was able to solve most of the problems that were pressing in his time

density matrix of a quantum system describes the possible polarization in a quantum sense. Consider two (orthogonal) quantum waves $|\psi_1\rangle$ and $|\psi_2\rangle$. These are called pure states. Additionally, two pure states can form a linear combination in superposition. In this case we find a density matrix with off-diagonal elements. From this point on, we denote the density matrix as $\rho(k, k')$ where k, k' denote quantum state[3]. $\rho = \sum_k p_k |\psi_k\rangle\langle\psi_k|$. We use the density matrix to The microcanonical ensemble assumes equal p_k for any two states k, k' with equal energy. We can rewrite this to any desired basis with the proper unitary transformation. The density matrix $\rho(k, k')$ includes the vital phase information in contrast to an ordinary density function $f(k)$.

4.3.1. Obtaining the density matrix

Let us start from the Hamiltonian of a closed system. A closed system has a limited energy and can therefore by described by a mathematically sound and compact H. This is a linear operator[4]. Following from equation 4.1, we find the Green's function for a closed quantum system [22].

$$G(z) = (z\mathbb{1} - H)^{-1}; z \in \mathbb{C} \tag{4.2}$$

The Hamiltonian has eigenfunctions which span the entire Hilbert space. Therefore we are allowed to expand G in eigenfunctions of H.

$$G(z) = \sum_j |\phi_j\rangle \frac{1}{z - \epsilon_j} \langle\phi_j| \tag{4.3}$$

This function diverges as z approaches ϵ_j. We introduce a imaginary term $i\eta$, where we let $\eta \downarrow 0$ to evaluate the equation 4.3 with complex function theory. $G^R(\epsilon) = (\epsilon\mathbb{1} - H + i\eta)^{-1}, \eta \downarrow 0$. ϵ is real, as the Hamiltonian is a Hermitian operator.
We try a general result from complex function theory, which states

$$\lim_{\eta \to 0} \frac{1}{x + i\eta} = \mathcal{P}\left(\frac{1}{x}\right) - i\pi\delta(x) \tag{4.4}$$

We combine equation 4.4 with the previous result of 4.3 to find:

$$\text{Im}G^R(\epsilon) = -\pi \sum_j |\phi_j\rangle \, \delta(\epsilon - \epsilon_j) \, \langle\phi_j|$$

We use the trace of a density matrix to extract the expectation value of any observable. Analogously, we take the trace of $\text{Im}G^R(\epsilon)$ to find the density of states (DOS):

$$\text{Tr Im}G^R(\epsilon) = \sum_i \langle\chi_i| \left(-\pi \sum_j |\phi_j\rangle \, \delta(\epsilon - \epsilon_j) \, \langle\phi_j| \right) |\chi_i\rangle = -\pi \sum_i \langle\chi_i| \left(\sum_j |\phi_j\rangle \, \delta(\epsilon - \epsilon_j) \, \langle\phi_j| \right) |\chi_i\rangle = -\pi \sum_j \delta(\epsilon - \epsilon_j) = -\pi$$

(4.5)

Where the summation over i cancels as one can pick any basis one like. Hence we choose the orthonormal basis created by eigenfunctions ϕ. This clever choice implies that $\langle\phi_i|\phi_j\rangle = 1$ if $i = j$ and zero in any other case.

4.3.2. DOS in a CISS experimental setup

With this result, we have shown how the density of states is related to the Greens function. In a CISS experiment, we apply a voltage difference to shoot the electrons through our chiral material. This bias is a strong force on the electrons and can be best described by a change in chemical potential. We use Fermi-Dirac statistics to obtain a reasonable model. On the one hand, this model suits non-interacting[5], identical particles that obey the Pauli exclusion principle (all fermions). On the other hand, it is easy in use, as the chemical potential is a explicit parameter of the Fermi-Dirac distribution.

[3] common denotion in any semi-classical approximation in condensed matter physics

[4] Proving H is a linear operator is a bit harder, but this result validates superposition in quantum mechanics, hence intuitively true

[5] Coulomb interactions between electrons have been widely researched within the theoretical field of CISS, but have not shown to be a significant force in the origin of the CISS effect

The distribution is a continuous function, but still strongly related to the density of states. Therefore we can find the following equation:

$$\int_{-\infty}^{\infty} \operatorname{Im} G^R(\epsilon) f_{\mathrm{FD}}(\epsilon, \mu)\, d\epsilon = -\pi\hat{\rho} \tag{4.6}$$

where f_{FD} is the Fermi-Dirac distribution:

$$f_{FD}(\epsilon, \mu) = \frac{1}{e^{(\epsilon-\mu)/k_B T} + 1} \tag{4.7}$$

4.4. NEGF: a matrix formalism

We still have to find a formulation for the Green's functions. In the previous section, we found the physical foundation for the Green's functions, and we found equations 4.5 and 4.6. These equations are our main result and we assume them to stay valid in our theory. However, the coupling to an electronbath implies that the Hamiltonian is no longer Hermitian. Firstly, we circle back to equation 4.2, our general case. For the Green's function, we take a still unknown Green's function G_S of the Green's function of our molecule, we use a function G_B for our electronbath, and these our coupled by a Hermitian function A. The following matrix can be substituted for $G(x, s)$ in equation 4.1. The formulation for substitute of $L(x)$ has a analogous approach. We use ϵ_a for the energy levels of the molecule, H_B for the Hamiltonian of the bath including the metallic leads between molecule and bath, and τ as a hopping parameter between the two sub-systems. These parameters form the Hamiltonian of our experimental setup, as we neglect the motion of the nucleus.[6] See the following matrices.

$$\mathcal{H} = \left(\begin{array}{c|c} \epsilon_a & -\tau \\ \hline -\tau^\dagger & H_B \end{array}\right) \qquad G = \left(\begin{array}{c|c} G_S & A^\dagger \\ \hline A & G_B \end{array}\right)$$

We still need to finalize our specific solution to 4.1 with the right delta function. The unit operator in the Hilbert space is a δ-function in position.[7]

$$\left(\begin{array}{c|c} z\mathbb{1}_S - H_S & -\tau \\ \hline -\tau^\dagger & z\mathbb{1}_B - H_B \end{array}\right)\left(\begin{array}{c|c} G_S & A^\dagger \\ \hline A & G_B \end{array}\right) = \left(\begin{array}{c|c} \mathbb{1}_S & 0 \\ \hline 0 & \mathbb{1}_B \end{array}\right) \tag{4.8}$$

We extract the following two equations:

$$(z\mathbb{1}_S - H_s)G_s + \tau A = \mathbb{1}_S \tag{4.9}$$

$$\tau^\dagger G_S + (z\mathbb{1}_B - H_B)A = 0 \tag{4.10}$$

Equation 4.9 is retrieved from the top left quadrant in the right hand side matrix of equation 4.8 , and 4.10 from the bottom left quadrant. We extract from 4.10 that $A = -(z\mathbb{1}_B - H_B)^{-1}\tau^\dagger G_S$, which is substituted in equation 4.9 to find the following expression:

$$G_s = (z\mathbb{1}_S - H_s - \Sigma)^{-1} \tag{4.11}$$

where

$$\Sigma = \tau g_B \tau^\dagger \text{ and } g_B = -(z\mathbb{1}_B - H_B)^{-1}.$$

[6] The motion of the nucleus is quantified in phonons and is part of the energy of the molecule, and therefore inherently part of the Hamiltonian. However, this does not play a role in electron transport.

[7] $\langle \underline{r} |\, \mathbb{1}\, | \underline{r}' \rangle = \delta(\underline{r} - \underline{r}')$

Σ is known as the self energy. Note that the self energy is a function of the hopping parameter. We denoted g_B for brevity. Furthermore, the self ernegy can be split in the real and imaginairy part, which is denoted as the following:

$$\Sigma = \Lambda - \frac{i}{2}\Gamma \tag{4.12}$$

We use this expression in the Schrödinger equation, to extract the meaning of both lambda en gamma. $\tilde{H} = H + \Sigma = H + \lambda - \frac{i}{2}\gamma$. This will result in the following superposition over time.

$$|\phi_j(t)\rangle = e^{(-it\tilde{\epsilon}_j - \gamma_j t/2)/\hbar}|\phi_j(t=0)\rangle \tag{4.13}$$

Where we see that γ_j is a real valued term in the solution, therefore our ϕ_j will exponentially decrease in amplitude over time. Thus γ represents the escape rate, in this particular case to the reservoir. λ represents a shift in energy. Now, we can use the definitions and results for the Green's functions in order to obtain an equation for the electron current. We first analyse the imaginary part of the retarded GF, which is essential for obtaining the density matrix:

$$\mathsf{Im}\, G^R = \frac{1}{2i}(G^R - G^A) = \frac{1}{2i}\left[(z\mathbb{1} - H + \Sigma)^{-1} - (z\mathbb{1} - H + \Sigma^\dagger)^{-1}\right] \tag{4.14}$$

$$\mathsf{Im}\, G^R(z) = \frac{1}{2i}\left[\frac{1}{z\mathbb{1} - H + \Sigma}\left(\frac{z\mathbb{1} - H + \Sigma^\dagger}{z\mathbb{1} - H + \Sigma}\right) - \left(\frac{z\mathbb{1} - H + \Sigma}{z\mathbb{1} - H + \Sigma^\dagger}\right)\frac{1}{z\mathbb{1} - H + \Sigma^\dagger}\right] \tag{4.15}$$

$$= \frac{1}{2i}\left[G^R\left(z\mathbb{1} - H + \Sigma^\dagger\right)G^A - G^R\left(z\mathbb{1} - H + \Sigma\right)G^A\right] \tag{4.16}$$

$$= \frac{1}{2i}\left[G^R\left(\Sigma^\dagger - \Sigma\right)G^A\right] \tag{4.17}$$

Here we have that $\Sigma^\dagger - \Sigma = i\Gamma$. Therefore,

$$\mathsf{Im}\, G^R(z) = \frac{1}{2}G^R(z)\Gamma G^A(z) \tag{4.18}$$

Now suppose we have two leads with self-energies Σ_S and Σ_D (S and D stand for 'source' and 'drain'). It is then straightforward to show that 4.15 still holds, but we substitute:

$$\Gamma = \Gamma_S + \Gamma_D. \tag{4.19}$$

To determine the current, we calculate the electron flow out of the source reservoir. By the conservation law of matter, we can find the current through the lead. The outflow is given by the charge in the source multiplied by the rate $\Gamma_s/\hbar$:

$$I^{\mathsf{out}}_{\mathsf{source}} = \frac{e}{\hbar}\mathsf{Tr}(\rho\Gamma_S) = \frac{e}{\hbar}\int \mathsf{Tr}\left[G^R\left(\Gamma_S f_S + \Gamma_D f_D\right)G^A\Gamma_S\right]d\epsilon \tag{4.20}$$

$$I^{\mathsf{out}}_{\mathsf{source}} = \frac{e}{\hbar}\int \mathsf{Tr}\left[G^R\left(\Gamma_S f_S + \Gamma_D f_D\right)G^A\Gamma_S(1 - f_S)\right]d\epsilon \tag{4.21}$$

As where the inflow denotes:

$$I^{\mathsf{in}}_{\mathsf{source}} = \frac{e}{\hbar}\int f_S\mathsf{Tr}\left[G^R\left[\Gamma_S(1 - f_S) + \Gamma_D(1 - f_D)\right]G^A\Gamma_S\right]d\epsilon \tag{4.22}$$

$$I_{\mathsf{source}} = I^{\mathsf{in}}_{\mathsf{source}} - I^{\mathsf{out}}_{\mathsf{source}} = \frac{e}{\hbar}\int \mathsf{Tr}\left[G^R\Gamma_D G^A\Gamma_S\right](f_S - f_D)d\epsilon = \frac{e}{\hbar}\int \mathcal{T}(\epsilon)(f_S(\epsilon) - f_D(\epsilon))d\epsilon \tag{4.23}$$

$\mathcal{T}(\epsilon)$ expresses the transmission in terms of couplings Γ and the advanced and retarded Green's function.

$$\mathcal{T}(\epsilon) = \mathsf{Tr}(G^R\Gamma_D G^A\Gamma_S) \tag{4.24}$$

4.5. The Büttiker probe

Up to now we have assumed that the molecule is coupled to the leads only. The transport is driven by the interactions between these leads and the molecule. In reality, there are interactions between the electrons on the molecule and between electrons and nuclei as well. These interactions -as well as interactions with phonons and defects- create phase-breaking and energy dissipation. Two terminal transport without electron interaction is coherent, implying that electrons can be described in terms of single-particle rather than many-body theory. Coherent transport obeys the Büttiker reciprocity, as seen in [26]. Büttiker reciprocity tells us that for a two-terminal system, time-reversal symmetry and unitarity of the scattering matrix (related to charge conservation) implies that the transport is symmetrical in the magnetisation, i.e. $\mathcal{T}_{RL}(m) = \mathcal{T}_{RL}(-m)$. Equation 4.23, shows that the symmetry holds for the current too. Recall the definition of the current polarisation:

$$P_{current} = \frac{I(m) - I(-m)}{I(m) + I(-m)} \tag{4.25}$$

Thus the Büttiker reciprocity does not allow for a magnetocurrent. Therefore we have to include electron interaction.
To create decoherence, i.e. dephasing of the electrons, we shall use a Büttiker probe following Bedkihal et al.[3]. The Büttiker probe allows for a general dephasing force, without a specified mechanism. Previous work has shown that electron-electron interactions do not play a significant role in the CISS effect. The general description of mesoscopic electron transport makes the Büttiker probe a suitable model. It contains a coupling to a third reservoir (in addition to source and drain) to which a zero net current flows in order to respect charge conservation. The charge on the molecule (which is the norm of the wave function of the electrons) is preserved, but phase information may not, allowing dephasing.

4.5.1. Büttiker reciprocity

The Büttiker probe is based on the Büttiker-Landauer formalism. Landauer found a formula for coherent electron transport on a mesoscopic scale. Büttiker expanded the theory by the introduction of terminals, where decoherence can be realised by one or more that do not carry a net current terminals by solving a finite sum over the Landauer equation. The equation has a transmission probability, which describes the electron scattering within the system, and a potential, which is related to the chemical potential. The chemical potential is a variable in the Fermi-Dirac equation, and thus contains the critical information about the available holes and electrons in the leads. Each terminal can be described as a separate reservoir. For a multi-terminal setup, the current through terminal ν is given by [3]:

$$I_\nu(m) = \int_{-\infty}^{\infty} d\epsilon \left(\sum_{\xi \neq \nu} \mathcal{T}_{\nu,\xi}(\epsilon, m) f_\nu(\epsilon) - \sum_{\xi \neq \nu} \mathcal{T}_{\xi,\nu}(\epsilon, m) f_\xi(\epsilon) \right) \tag{4.26}$$

Within this formalism, a Büttiker probe is a terminal with zero net current: the chemical potential of the probe is such that the inflow into the reservoir from terminals of higher chemical potential is equal to the outflow to terminals of lower chemical potential. Electrons can move against the potential driven by scattering processes, which are accounted for within the Landauer-Büttiker formalism.

When including Büttiker probes into our formalism, we only make two assumptions. Firstly, assume that the transmission between two reservoirs obeys reciprocity, as we would like the unitarity and time reversal symmetry of the scattering matrix to hold [3]:

$$\mathcal{T}_{\xi,\nu}(\epsilon, m) = \mathcal{T}_{\xi,\mu}(\epsilon, -m) \tag{4.27}$$

Furthermore, the total probability must be conserved,

$$\sum_{\xi \neq \nu} \mathcal{T}_{\xi,\nu}(\epsilon, m) = \sum_{\xi \neq \nu} \mathcal{T}_{\nu,\xi}(\epsilon, m). \tag{4.28}$$

as a result of the Green's function formalism. This is also true after the implementation of the probe, see Appendix A of reference [16].

Combining these assumptions, we find the expression for the currents. We take the subscripts L and R for the left and right lead respectively, and P for the Büttiker probe. The current through the left lead is given by:

$$I_L(m) = \int_{-\infty}^{\infty} d\epsilon \left(T_{L,R}(\epsilon, m) f_L(\epsilon) - T_{R,L}(\epsilon, m) f_R(\epsilon) + T_{L,P}(\epsilon, m) f_L(\epsilon) - T_{P,L}(\epsilon, m) f_P(\epsilon, m) \right). \quad (4.29)$$

For the net zero current through the probe, we find:

$$I_P(m) = \int_{-\infty}^{\infty} d\epsilon \left(T_{P,L}(\epsilon, m) f_P(\epsilon) - T_{L,P}(\epsilon, m) f_L(\epsilon) + T_{P,R}(\epsilon, m) f_P(\epsilon) - T_{R,P}(\epsilon, m) f_R(\epsilon) \right). \quad (4.30)$$

4.5.2. Büttiker reciprocity for a multi-terminal setup

The self-energy is physically explained from two sources: either interaction with the leads or phase-breaking within the helicene molecule. Adding a büttiker probe does not change our molecule, but it offers another reservoir for electrons, which must be treated as a lead. By, those equations, we denote the following equation:

$$\Sigma = \Sigma_\phi + \sum_p \Sigma_p \quad (4.31)$$

The Σ_ϕ arises from the leads (and is not part of the molecular Hamiltonian) and the sum over the leads p.[8].

As seen in equations 4.14 through 4.18, the linearity of the of the self energy is preserved in terms of the scattering rate Γ. We can extend this result to any number of terminals, where the transmission from terminal p to q is given by:

$$\mathcal{T}_{pq} = \frac{e}{\hbar} \int \mathrm{Tr} \left[\Gamma_p G^R \Gamma_q G^A \right] (f_p - f_q) d\epsilon \quad (4.32)$$

4.6. Summary and Conclusion

Non-equilibrium Green's functions allow us to describe the interaction between the molecule and two semi-infinte electron baths connected as terminals. We have found the Meir-Wingreen formula to describe transport in such systems. Moreover, it is possible to extend this formalism with a Büttiker probe, which creates the necessary decoherence which is inherent to electron transport on mesoscopic scale. Later on, this will allow us to measure a magnetocurrent in the experiment.

[8] The helicene model is a non-interacting model. The electrons are treated as independent waves or particles. This part of the self-energy arises as electrons scatter of each other. This is not allowed within the model

5

The 6-Helicene model

For our symmetry analysis, we take the model of a 6-helicene molecule described by Geyer [9]. Helicene is a relative simple molecule -only carbon and hydrogen bonds are present- with a helix lay-out, see figure 2.1. Previous work found the CISS effect in monolayers of helicene [15], and the simple structure makes it a perfectly suited molecule for a model. The model is based on perturbation theory, which revealed that different components of the spin orbit coupling contribute with different weights to the CISS effect. Mesoscopic electron transport is key in tuch experiment. Therefore, we need an Hamiltonian on atomic level, which provides all the information on the quantum nature of the molecule, or to be more precise, the electronic nature of the molecule as well as the spin-orbit interaction. Transport calculations are included through a simplified continuous version of a tight-binding model and show that under certain conditions spin polarisation can be maintained.

5.1. Geometry of the model

The chiral nature of 6-helicene can be decomposed into three concentric helices. The carbon atoms lay on radius, a_0, $2a_0$ and $a_1 = \sqrt{7}a_0$ with increasing magnitude. a_0 is the length of the hexagon sides, measured at 1.4 Å for two carbon atoms, as a result of their orbital interaction. This implies that two neighbouring atoms in the inner cylinder are separated over an angle $\frac{2\pi}{6} = \frac{\pi}{3}$. In the outer helix, two neighbouring atoms are separated over $\phi_2 = 2\arcsin(1/(2\sqrt{7})) \approx 21.8°$. Neighbouring atoms over the middle and outer cylinder are separated over $\phi_1 = 1/2(\pi/3 - \phi_2 \approx 19.1°$. See figure 5.1 for a schematic overview of the xy-projection of the helicene model. Given this compact set of parameters, we can describe the all the carbon atoms by one position vector:

$$\underline{R}_i = \left(R_i \cos\Phi_i, \quad R_i \sin\Phi_i, \quad \frac{b}{2\pi}\Phi_i \right) \tag{5.1}$$

The *capital* Φ represents any sum of multiples of ϕ_0, ϕ_1 and ϕ_2. Figure 5.1 gives a visual representation, and can provide critical inside on the construction of Φ. R_i is one of the three mentioned radii describing the position of the carbon atoms. The parameter b appears in the expression of the z-coördinate, and gives the height of one full rotation around the helixal axis. The parameter b is modelled with r_0. This is a useful tool, as the symmetry of the tetrahedral molecular geometry allows us to consistently express the position along the x-axis as function of r_0.

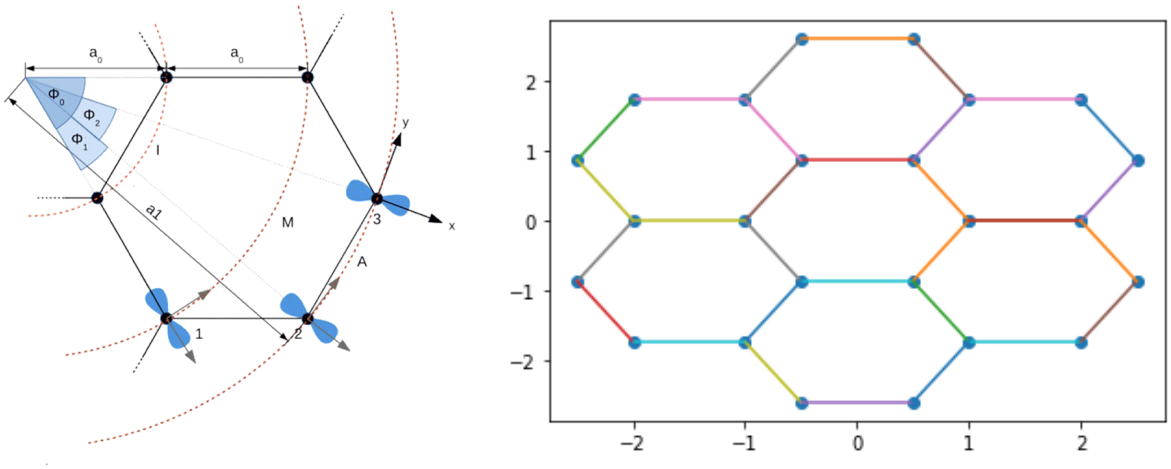

Figure 5.1: A schematic overview of the projection of the helical model in the xy-plane with the defined geometrical parameters. On the right (adapted from [9]), the inner(I), middle(M) and outer(A) cylinders are depicted with dashed circles. The blue hourglasses represent the orientation of selected orbitals. On the right, a Python figure, made with the library Matplotlib, of the model in a xy-plane projection as it is used in this thesis.

5.2. The electronic Hamiltonian and the Slater-Koster formalism

A carbon atom contains six electrons, two of which occupy an s-orbital at low energy (about -15 eV). The remaing four are in so-called 'hybridized' orbitals which are linear combinations of s- and p- orbitals. In the helicene molecule, the carbon atoms are SP2-hybridized. In this hybridization, three electrons participate in chemical bonds with neighbouring carbon atoms lying in a plane at angles of 120°. Perpendicular to this plane, a p_z orbital hosts an electron at higher energy than the in-plane bonds. The p_z orbitals are responsible for electron transport. A Slater-Koster (SK) Hamiltonian is a good approximation to the independent particle Hamiltonian. The following table gives the matrix elements used in the SK approximation:

$V_{ss\sigma}$	-7.92 eV
$V_{sp\sigma}$	8.08 eV
$V_{pp\sigma}$	7.09 eV
$V_{pp\pi}$	-3.44 eV
ϵ_σ	-18 eV
$\epsilon_{p\sigma}$	-18 eV
$\epsilon_{p\pi}$	-10.5 eV

Table 5.1: The Slater-Koster parameters and on-site energies that were used in the model.

These parameters of the Slater-Koster formalism are listed below:

1. $V_{ss\sigma}$ describes the boundedness between two s orbitals
2. $V_{sp\sigma}$ describes the boundedness between a s and a p orbital
3. $V_{pp\sigma}, V_{pp\pi}$ describes the different boundednesses between two p orbitals.

These potentials can be calculated, which results in the following table:

The ϵ-parameters describe the energy of the electron in the atomic orbital described by its subscript. ξ_p is a parameter of particular interest in our study of the CISS effect. It represents the spin-orbit coupling constant. We'll see more on this parameter later on.

5.2.1. The onsite Hamiltonian

We construct the Hamiltonian for a single atom affected by perturbations along the SK formalism as follows:

$$h^{(i)} = \begin{pmatrix} \epsilon_s & 0 & 0 & 0 \\ 0 & \epsilon_{p\sigma} & -i\sigma_z\xi_p & i\sigma_y\xi_p \\ 0 & i\sigma_z\xi_p & \epsilon_{p\sigma} & -i\sigma_x\xi_p \\ 0 & -i\sigma_y\xi_p & i\sigma_x\xi_p & \epsilon_{p\pi} \end{pmatrix}$$

On the diagonal, we find the potential of the orbitals as expected. Off-diagonal elements arise as a result of the spin-orbit coupling, where the spin of an electron interacts with its motion in the atomic orbital. We neglect the effect of external electric fields. Previous research including graphene nanotubes found the SOC-constant ξ_p to be around 6 meV. This research includes effects of the curvature in a helix and the hexagonal nature of helicene, see reference [13]. This paper proves that calculations on the intra-atomic[1] Hamiltonian can show that spin-flip is allowed, essential for the CISS effect.
The transfer Hamiltonian uses the SK formalism as well. Geyer and Visscher successfully implemented this in their model. Since this is not the focus of this thesis, the details of the transfer Hamiltonian can be found in Appendix A.4

5.3. Transmission, current and Büttiker probe optimisation

Privously in this chapter, we described the SK Hamiltonian as model for our experiment. Chapter 4 showed us how to use the Hamiltonian to find the associated Green's functions essential to formulate transport between two terminals. This model was implemented by M. Visscher, based on the paper by Geyer. See reference [23] for her work on the CISS effect and the Breit interaction. Moreover, we came to the conclusion that a Büttiker probe can be used to incorporate decoherence which is necessary to obtain a magnetocurrent. The net current through the Büttiker probe must be zero. This would imply that we have the Büttiker probe as a third terminal at a potential which we tune such that the net current into the probe vanishes. See equation 4.32. We solve this equation for μ given $I_{BP} = 0$. We find the following root finding problem for μ_P:

$$I_{BP} = \int_{-\infty}^{\infty} d\epsilon \left[T_{P,L}(\epsilon)f_P(\epsilon,\mu_P) - T_{L,P}(\epsilon)f_L(\epsilon,\mu_L) + T_{P,R}(\epsilon)f_P(\epsilon,\mu_P) - T_{R,P}(\epsilon)f_R(\epsilon,\mu_R)\right]. \quad (5.2)$$

We discretise the integral over all ϵ within the bias voltage range, i.e. $-V/2 < \epsilon < V/2$. We solve for mu_P for a sequence of bias voltages V. The sequence of μ_P's can be used to determine the current at every voltage. Where we solve the integral of equation 4.32 discretely with a Riemann sum with interval length $V/400$. Finally, we calculate the current for every spin we can establish the success or lack of it.

This addition makes it quite straightforward what our main concern must be: we need to understand the effect of the Büttiker probe. We shall analyse the result in twofold. First, we take a look at the rotational symmetries. We define the system, its rotational axes, and we look at the theoretical result of the current polarisation. Secondly, we take a look at the anisotropy of the Büttiker probe. Its decoherence might prove to be a key element of the current polarisation. We use the projection matrices in appendix A.5 to orient both the magnetisations as well as the Büttiker probe in the desired direction.

[1] The Hamiltonian that contains the information of the atom itself, not the information on the interaction with its surroundings.

6

Results and symmetry analysis

Recall that the **system** is defined as the helicene molecule. In chapter 4, we described how the system interacts with the surroundings: the leads and the Büttiker probe (BP). We use a coordinate system where the z-axis is the axis along the length of the molecule, see figure 6.1. In the following paragraphs, we analyse the results for the current difference and polarisation for different magnetisations.

6.1. Magnetisation along the x-axis

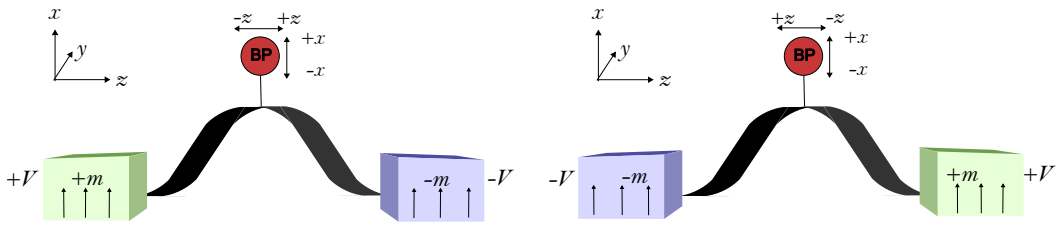

Figure 6.1: The experimental setup before and after a rotation of π radians around the x-axis. Note that the orientation of the Büttiker probe does not change as we rotate.

Symmetry analysis

The system is invariant under rotation around the x axis about π. The contact however, are exchanged, resulting in $+m \rightarrow -m$. Furthermore, the exchange of the leads inverts the voltage. This means that the electrons reverse their direction and therefore the current changes sign. In this respect, the rotation is like a time-reversal.
Besides the change in momentum, the rotation results in the following transformation:

$$x \rightarrow x, y \rightarrow -y \text{ and } z \rightarrow -z. \tag{6.1}$$

We find the change in angular momentum to be:

$$\underline{L} = \begin{pmatrix} yp_z - zp_y \\ -zp_x + xp_z \\ -xp_y + yp_z \end{pmatrix} \rightarrow \begin{pmatrix} L_x \\ -L_y \\ -L_z \end{pmatrix} \tag{6.2}$$

.

As spin $\underline{S}$ is angular momentum too, this rotation does not effect the orientation of the SOC, which scales with $\underline{L} \cdot \underline{S}$. Therefore we can conclude that the SOC is invariant for this rotation. Moreover, for the Büttiker probe oriented along the x-axis, we have that $S_x \rightarrow S_x$. We can summarize this analysis in the following equation:

$$I(V, m, BP_x) = -I(-V, -m, BP_x) \tag{6.3}$$

Results of the model

We set the maximum potential to 1.5, we take k_BT to be 0.02, and the discretization for the energies and the experimental bias to be $V_{max}/400$, as described previously. This is merely the resolution of the grid and of our measurement. The number of data points, thus the number of applied voltages, is 1/5th of the grid resolution. We find the following current difference:

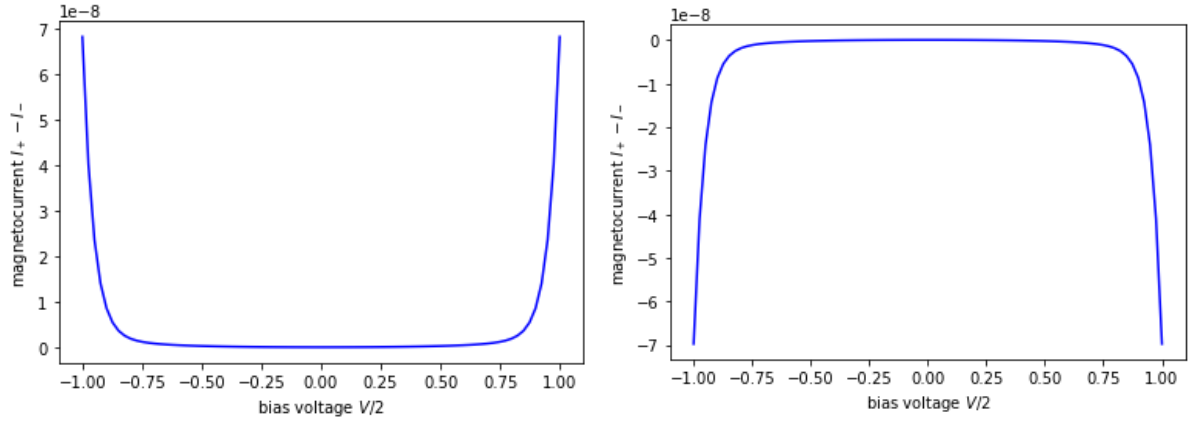

(a) The Büttiker probe aligned with the left lead before rotation and the right lead after rotation; (BP_{+x})

(b) The Büttiker probe aligned with the right lead before rotation and the right lead after rotation; (BP_{-x})

Figure 6.2: Results for the current difference for polarisation of the Büttiker probe along the x-axis.

In another experimental setup, we orient the BP along the z-axis. We take a look at the current difference in experiments analogue to those above. The results are shown in the figure below:

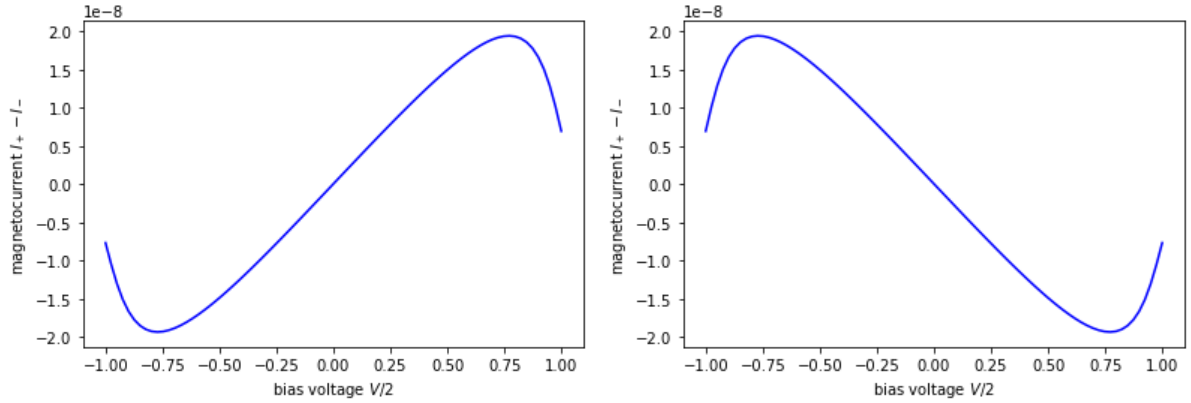

(a) The BP aligned with the along the positive z axis; BP_{+z}

(b) The BP aligned along the negative z-axis; BP_{-z}

Figure 6.3: Results for the current difference for polarisation of the Büttiker probe along the positive and negative z-axis, respectively

The results for BP_z are inverted, similar to BP_x. A key difference shows, when studying the Büttiker probe more closely. When we align it along the +z-axis, and we rotate our system, including the fixed probe, we notice that the transformation is a bit different. A rotation of π rad around the x-axis inverts the alignment of the BP:

$$I(V, m, BP_z) = -I(-V, -m, -BP_z) \tag{6.4}$$

At first glance, the current polarisation poses a more problematic result:

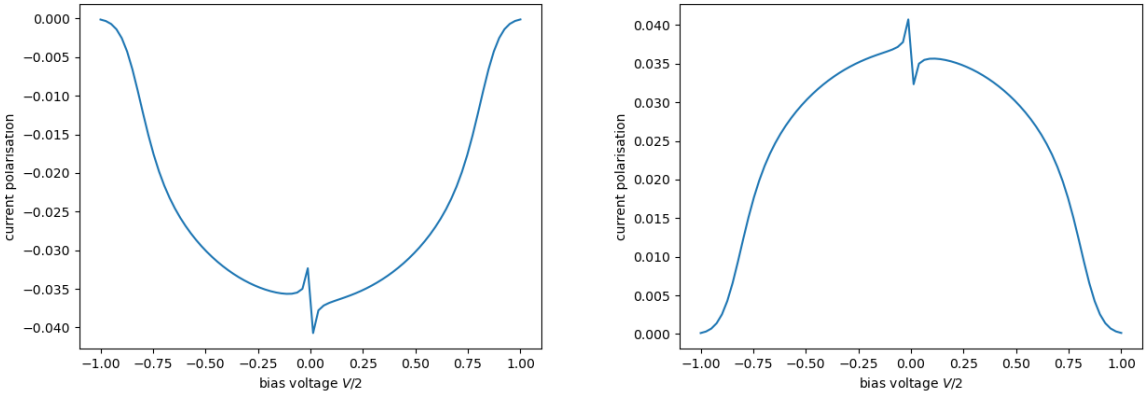

(a) The BP aligned with the along the positive z axis; BP_{+z}

(b) The BP aligned along the negative z-axis; BP_{-z}

Figure 6.4: Results for the current difference for polarisation of the Büttiker probe along the positive and negative z-axis, respectively

The results above show a remarkable result around zero bias. There are two possible causes for numerical errors:
1. The integral limits are not entirely outside the molecular spectrum.
2. There is a finite interval size in the integrations.
Both options are considered in the analysis.

Analysis of the results

The transformation in equation 6.1 results in $I(V, m, BP) = -I(-V, -m, \tilde{BP})$, where $\tilde{BP}$ denotes the transformed value of the Büttiker probe. Consider:

$$I(V, m, BP) - I(V, -m, \tilde{BP}) = \Delta I.$$

Time reversal symmetry tells us that $I(V, m, BP) = -I(-V, m, BP)$. Please note that this magnetisation does not change, since we have purely a magnetisation as a result of a fixed ferromagnet, which specifically breaks time reversal symmetry as a result of the experimental setup. The ΔI stated above is the difference between two magnetisations. Moreover, the BP creates a decoherence. Based on the antisymmetric results in both figure 6.2 as well as in figure 6.3, we conjecture a linear We combine the statement above with the knowledge thah

$$\Delta I(V, m, BP) = -\Delta I(V, m, -BP) \tag{6.5}$$

Case 1: $\tilde{BP} = BP$
This is the case when the BP is oriented along the x-axis.

$$\begin{aligned} \Delta I(V, m, BP) &= I(V, m, BP) - I(V, -m, BP) \\ &= -I(-V, -m, BP) + I(-V, m, BP) \\ &= \Delta I(-V, m, BP); \end{aligned} \tag{6.6}$$

concluding that ΔI is symmetric in V.

Case 2: $\tilde{BP} = -BP$
This is the case when the BP is oriented along the z-axis.

$$\begin{aligned} \Delta I(V, m, BP) &= I(V, m, BP) - I(V, m, BP) \\ &= -I(-V, -m, -BP) + I(-V, m, -BP) \\ I(-V, -m, BP) - I(-V, m, BP) &= -\Delta I(-V, m, BP) \end{aligned} \tag{6.7}$$

Here we conclude that ΔI is antisymmetric in V as well.

6.1.1. An isotropic Büttiker Probe

Expanding on our conjecture, we take a look at the isotropic BP. In this case, an inversion of the current so ΔI must be zero. We take a look at the result in our regular defintion of 401 points, and we take a better look at 1601 integration points:

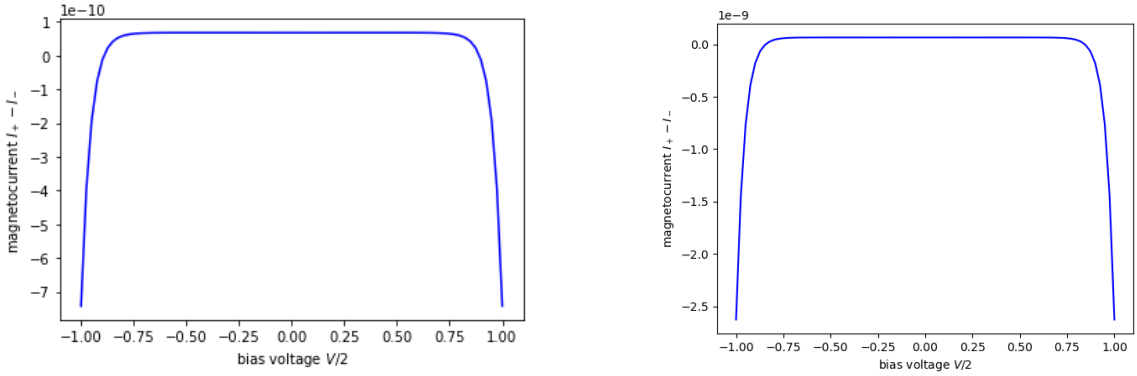

Figure 6.5: Results for the current difference for an isotropic Büttiker probe, modeled with 401 and 1601 integration points at the bias axis, respectively.

We inmediately notice the value on the y-axis, the current difference is very small. This can be the result of numerical errors. The improved resolution does not raise additional concerns around small bias voltages. However, the tails at high bias voltage are increased in size. We conjecture that the nonzero current difference is due to the fact that at the boundaries of the interval, the transmission is not exactly zero. The transmission at extreme bias are shown in the figure below:

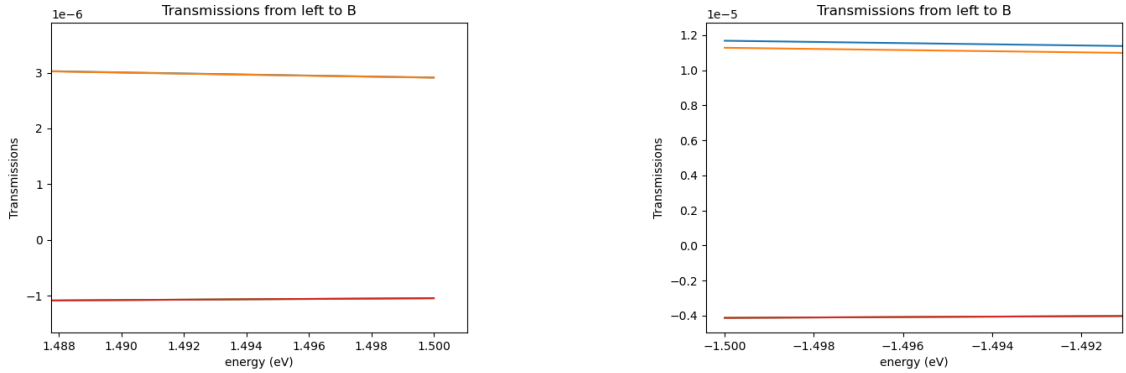

Figure 6.6: Transmission from the left lead to the Büttiker probe at maximum and minimum bias, respectively.

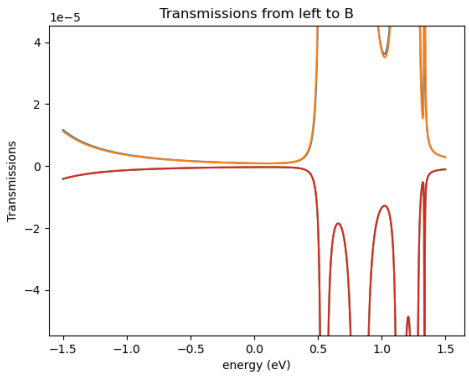

Figure 6.7: A detailed readout from the transmission from the left lead to the Büttiker probe at a magnitude of order 10^{-4}

6.2. Magnetisation along the z-axis

This is the case as it is analysed by Rikken [20].

Büttiker probe oriented along the x-axis

In another experimental setup, we magnetize the leads along the z-axis, which is the helical axis of the molecule, see figure 6.9 for a schematic overview of the experiment.
We analyse the symmetry properties for different Büttiker probes. We rotate around the x-axis. In both situations, the magnetisation points towards the system from both sides. The source and drain swap positions, thus $V \Rightarrow -V$. For the viewer, the magnetisation remain uneffected; only the bias changed sides. This difference is clearly visible in the current difference.

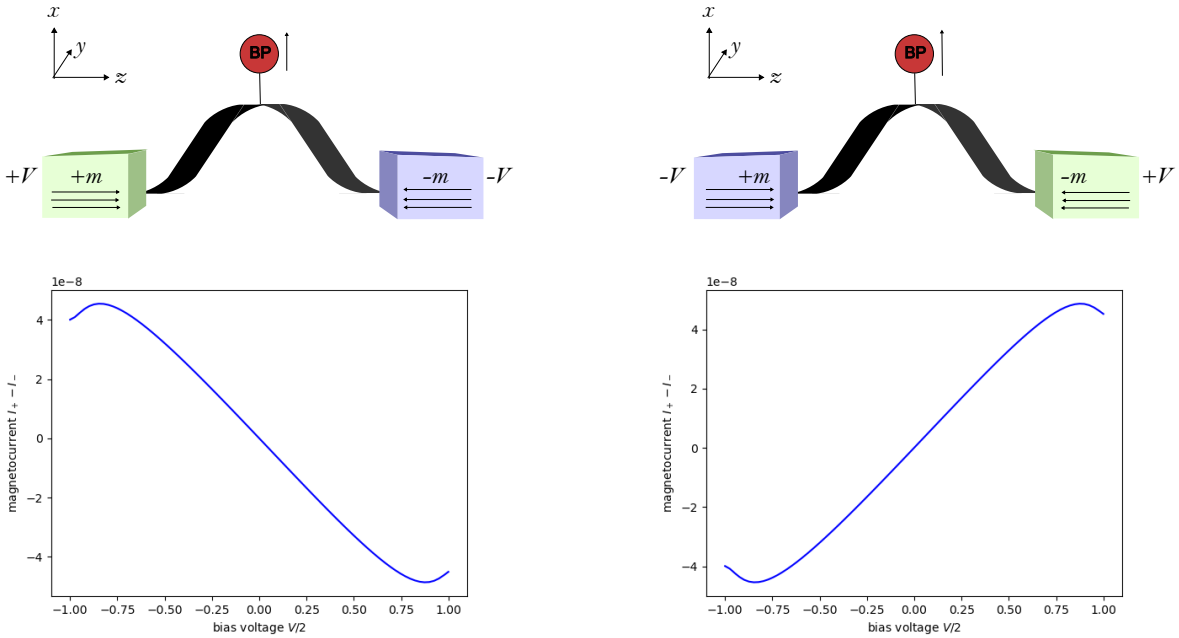

Figure 6.8: From top to bottom the experimental setup, the current difference, and current polarisation for magnetization along the z-axis. We have on the left the original, on the right the results after a rotation of π rad around the x-axis.

In the upper two images, it is clearly visible that the rotation around the x-axis does not change the Büttiker probe orientation. The inversion of the bias voltage leads to an inversion of the current difference in accordance with our conjecture.

Büttiker probe along the z-axis

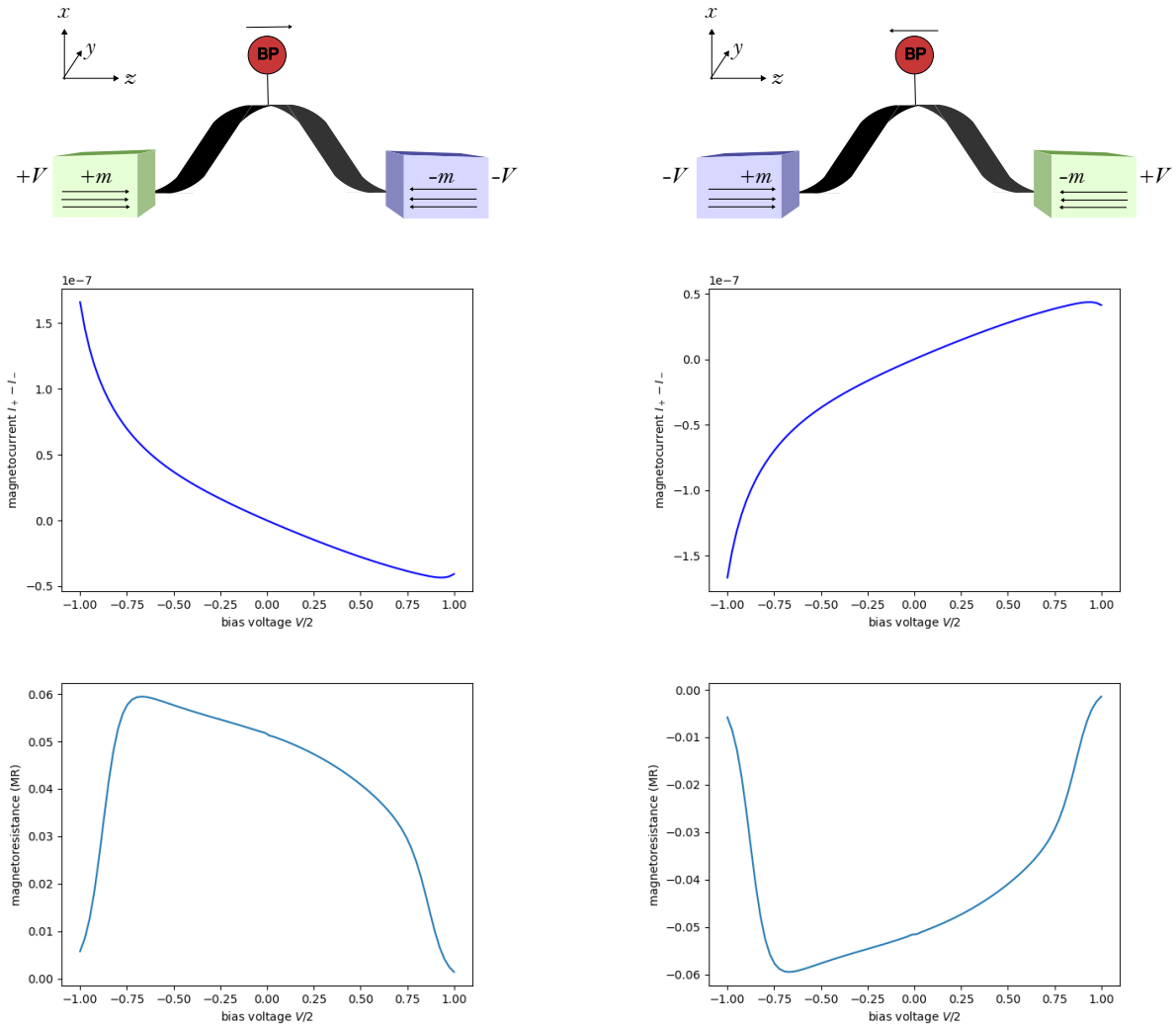

Figure 6.9: From top to bottom the experimental setup, the current difference, and current polarisation for the leads magnetized along the z-axis. We have on the left the original, on the right the results after a rotation of π rad around the x-axis.

When we rotate around the z-axis. There is no apparent change for the device or the magnetisation. There is no useful conditional rotation around x; such rotation would invert the sign of the BP, but both V and I flip sign as well. Thus the results do not show a clear (anti)symmetry.
In summary, a rotation around x,y,z does not change the device. We cannot expect any specific behaviour. It is important to note that one specific setup, including the magnetisation of the leads, will lead to an antisymmetric IV curve.

6.2.1. Isotropic Büttiker probe

An isotropic Büttiker probe would not allow for a current difference. The argument made in the previous section holds independent from the applied magnetisation. In the figure below, we see that indeed find a data set that suggest numerical errors and interference at the boundaries of the interval. The order 10^{-11} is not related to any of the modelled influences, such as the magnetisation and bias voltage. The different lengths of the tails might suggest interference from outside the interval. We conjecture that the anisotropy of the Büttiker probe does not allow for a current difference.

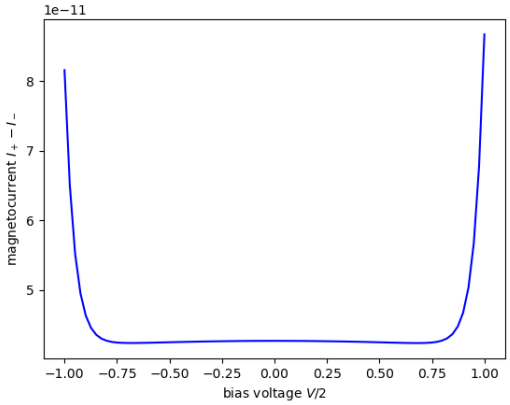

Figure 6.10: The current difference for an isotropic Büttiker probe with lead magnetisation along the x-axis.

7

Conclusion & Discussion

This thesis explores the symmetries of the IV characteristics observed in the CISS effect, in particular the effect of different magnetisations and of different orientations for the Büttiker Probe. This probe is a key element to mimic the decoherence in electron transport. The magnetisation of the leads was both taken along the x-axis as well as the z-axis. In both the scenarios, we aligned the probe along different axes, as well as an isotropic probe.
Our research objective was sparked by previous research by Rikken. He claims in reference [20]:
*(..) it should be noted that for symmetrical devices, magnetic field dependent antisymmetric **I-V** curves (..) are unphysical, as a simple rotation over 180° around an axis perpendicular to the current leaves the device unchanged but inverts the direction of the magnetisation. We must therefore conclude that device asymmetry is a necessary condition for antisymmetric **I-V** curves (..).*
With the implementation of the Büttiker probe, we were able to formulate a conjecture, which implies agreement with the claim by Rikken. Implementing an asymmetry by orienting the Büttiker probe along or perpendicular to the magnetisation shows antisymmetric IV curves. After the research described in this thesis, we find the conjecture that $\Delta I(V, m, BP) = -\Delta I(V, m, BP)$. This denotes that the $I - V$ curves resulting from two terminal CISS experiments have a linear relation to the decoherence created by the Büttiker probe. This is analogous to stating that the $I - V$ curves have a linear dependency on the perturbations in the device.
Isotropic Büttiker probes show no antisymmetric $I - V$ curves. We conjecture that the very small MR observed for the isotropic BP is due to numerical errors. Further research into this issue is needed.

Future research

The changeable nature of the electron transmission could be of influence to discontinuity in the current polarisation. Further numerical analysis, preferably with a finer integration grid, is required to rule out any errors and further develop the conjecture above. The nature of a rotation around the y-axis is an interesting topic which might shine more light on how the perturbations in the device affect the realisation of the CISS effect.

References

[1] Matteo Atzori et al. “Magneto-chiral anisotropy: From fundamentals to perspectives”. In: *Chirality* 33.12 (2021), pp. 844–857.

[2] Laurence D Barron. “Fundamental symmetry aspects of molecular chirality”. In: *New developments in molecular chirality*. Springer, 1991, pp. 1–55.

[3] Salil Bedkihal, Malay Bandyopadhyay, and Dvira Segal. “The probe technique far from equilibrium: Magnetic field symmetries of nonlinear transport”. In: *The European Physical Journal B* 86.12 (2013), p. 506.

[4] AD Benoit et al. “Asymmetry in the magnetoconductance of metal wires and loops”. In: *Physical review letters* 57.14 (1986), p. 1765.

[5] M Buttiker. “Symmetry of electrical conduction”. In: *IBM Journal of Research and Development* 32.3 (1988), pp. 317–334.

[6] M Büttiker. “Four-terminal phase-coherent conductance”. In: *Physical review letters* 57.14 (1986), p. 1761.

[7] S. Datta. *Electronic Transport in Mesoscopic Systems*. Cambridge Studies in Semiconductor Physi. Cambridge University Press, 1997. ISBN: 9780521599436. URL: https://books.google.nl/books?id=28BC-ofEhvUC.

[8] “Field-Dependent Green Functions”. In: *Quantum Kinetics in Transport and Optics of Semiconductors*. Berlin, Heidelberg: Springer Berlin Heidelberg, 2008, pp. 115–156. ISBN: 978-3-540-73564-9. DOI: 10.1007/978-3-540-73564-9_10. URL: https://doi.org/10.1007/978-3-540-73564-9_10.

[9] Matthias Geyer et al. “Chirality-induced spin selectivity in a coarse-grained tight-binding model for helicene”. In: *The Journal of Physical Chemistry C* 123.44 (2019), pp. 27230–27241.

[10] Josiah Willard Gibbs. *Elementary Principles in Statistical Mechanics: Developed with Especial Reference to the Rational Foundation of Thermodynamics*. Reprint of the original 1902 edition published by Yale University Press. New York: Dover Publications, 1960.

[11] B Göhler et al. “Spin selectivity in electron transmission through self-assembled monolayers of double-stranded DNA”. In: *Science* 331.6019 (2011), pp. 894–897.

[12] David J Griffiths and Darrell F Schroeter. *Introduction to quantum mechanics*. Cambridge university press, 2018.

[13] Daniel Huertas-Hernando, Francisco Guinea, and Arne Brataas. “Spin-orbit coupling in curved graphene, fullerenes, nanotubes, and nanotube caps”. In: *Physical Review B—Condensed Matter and Materials Physics* 74.15 (2006), p. 155426.

[14] KH Huisman. “Theory of Chirality Induced Spin Selectivity in Two Terminal Transport”. PhD thesis. Delft University of Technology, 2023.

[15] Vankayala Kiran et al. “Helicenes—A new class of organic spin filter”. In: *Advanced Materials* 28.10 (2016), pp. 1957–1962.

[16] Toshihiro Kubo, Yuki Ichigo, and Yasuhiro Tokura. “Phase and amplitude of Aharonov-Bohm oscillations in nonlinear three-terminal transport through a double quantum dot”. In: *Physical Review B—Condensed Matter and Materials Physics* 83.23 (2011), p. 235310.

[17] Anneli Löfgren et al. “Symmetry of two-terminal nonlinear electric conduction”. In: *Physical review letters* 92.4 (2004), p. 046803.

[18] DA Papaconstantopoulos and MJ Mehl. “The Slater–Koster tight-binding method: a computationally efficient and accurateapproach”. In: *Journal of Physics: Condensed Matter* 15.10 (2003), R413.

[19] K Ray et al. “Asymmetric scattering of polarized electrons by organized organic films of chiral molecules”. In: *Science* 283.5403 (1999), pp. 814–816.

[20] GLJA Rikken and N Avarvari. “Comparing electrical magnetochiral anisotropy and chirality-induced spin selectivity”. In: *The journal of physical chemistry letters* 14.43 (2023), pp. 9727–9731.

[21] Daniel V. Schroeder. *An Introduction to Thermal Physics*. Illustrated. San Francisco, CA: Addison Wesley, 2000. ISBN: 9780321277794.

[22] Johannes S. Seldenthuis and Joseph M Thijssen. “Understanding transport through molecular orbitals”. In: ().

[23] Marieke Visscher. “The effect of the Breit interaction on Chirality Induced Spin Selectivity”. Msc thesis. Leiden University, 2022.

[24] DH Waldeck, R Naaman, and Y Paltiel. “The spin selectivity effect in chiral materials”. In: *APL materials* 9.4 (2021).

[25] Xu Yang. “Connecting chirality and spin in electronic devices”. PhD thesis. University of Groningen, 2020.

[26] Xu Yang, Caspar H. van der Wal, and Bart J. van Wees. “Spin-dependent electron transmission model for chiral molecules in mesoscopic devices”. In: *Phys. Rev. B* 99 (2 Jan. 2019), p. 024418. DOI: 10.1103/PhysRevB.99.024418. URL: https://link.aps.org/doi/10.1103/PhysRevB.99.024418.

A

Extended information about the physical mechanisms.

A.1. Quantum mechanics, a mathematical approach

For readers without an extended background in the field of physics, the quantum mechanical world can be a frightening one. Quantum mechanics are confusing, abstract and counter intuitive. However, when we accept the needed mathematical tools essential to the field of quantum mechanics, the approach can be as straightforward as its results are surprising.
Hamiltonian mechanics describes the physical world through the same principles as Newton introduced, but it uses different tools and has different applications. Newtonian physics is a description of mechanics in terms of forces, where Hamilton focused on the energies in play. It started with the work of Joseph-Louis Lagrange and his introduction of the langrangian: $\mathcal{L} = \mathcal{T} - \mathcal{V}$, which uses the stationairy-action principle. This principle offers an alternative way to look at dynamics. Newton and his invention of calculus relies heavily on vector field calculations: two forces can cancel each other *given they act in opposite directions*. However, in Langrangian mechanics, one expresses all actions in general coordinates and their respective angles. This enables us to come up with the same results without the use of vectors. This turns out to be a vital asset as we do our quantum wave calculations in a Hilbertspace, where the definition of a distance is different from the human concept of distance. Sir Hamilton denoted the Hamiltonian as $\mathcal{H} = \mathcal{T} + \mathcal{V}$, the sum of kinetic en potential energy. In quantum mechanics, we can further simplify this definition to any kind of energy, as the dynamics work a little differently. In quantum mechanics, the Hamiltonian is an operator on the quantum, and solving the associated eigenvalue problem, $\mathcal{H}\psi = E\psi$ solves for the energy of the quantum wave. With the introduction of linear and higher order perturbations on basic and analytic solvable eigenvalue problems, we can solve for a wide variety of quantum problem. This is called perturbation theory is the root of the Slater-Koster formalism used in our model.

A.2. Spin orbit coupling

To understand the basic idea of spin-orbit coupling (SOC), we use a classical[1] approach [12]. Take a **spinning**, i.e. rotating around an internal axis, electron in orbit around an atomic nucleus. From the perspective of the electron, the nucleus orbits around the electron. The *moving* charge from the nucleus creates a magnetic field in the electron restframe[2]. The magnetic dipole of the electron tends to line out in the direction of the magnetic field, similar to a compass following the direction of any nearby magnetic field lines. This results in the Hamiltonian given by

$$\mathcal{H}_{SOC} = -\mu_{electron} \cdot B_{proton} \tag{A.1}$$

[1] i.e. we stay away from all dualities and uncertainty principles

[2] This restframe is **not** Galilean invariant, the electron accelerates constantly towards the nucleus, therefore we find no inertial system. We can account for the mathematical error by constantly changing from inertial system using Lorentz transformations . This technique is known as the *Thomas precession.*

For the magnetic field created by the proton, we assume that the orbiting proton acts as a continuous current loop[3]. A current loop of radius r creates a magnetic field in its middle point with magnitude according to Biot-Savart's law:

$$B = \frac{\mu_0}{4\pi} \int_C \frac{Id\ell \times \hat{r}}{r^2} = \frac{\mu_0 I}{2r} \tag{A.2}$$

As electronic current is truly the charge passing by in a certain time, we use that the proton takes one orbital period to pass by with an elementary charge, so $I = e/T$.
Now we look at the situation from the restframe of the nucleus. In this frame, the angular momentum of the electron can be described as $L = mvr = 2\pi mr^2/T$. We also notice that $\underline{B}$ and $\underline{L}$ point in the same direction. Thus we can express $\underline{B}$ in terms of $\underline{L}$.

$$\underline{B} = \frac{1}{4\pi\epsilon_0} \frac{e}{mc^2 r^3} \underline{L} \tag{A.3}$$

For the magnetic dipole moment of the electron, we use classical electrodynamics. We take electron charge e evenly spread out of a ring of radius r. The ring rotates with period T. Magnetic dipole moment is the current times the area, resulting in:

$$\mu = \frac{e\pi r^2}{T} \tag{A.4}$$

The mass of the ring is m, so its inertia is mr^2, multiplied by the angular velocity, resulting in a classical angular momentum: $\underline{S} = 2\pi mr^2/T$. Using the gyromagnetic ratio μ/S, we find the following expression for all object with even distribution of mass densities and currents:

$$\mu = \frac{e}{2m} \underline{S} \tag{A.5}$$

We can put everything together to find an expression for the SOC. However, we still have to factor in all quantum related physics. Dirac's theory found a correction of 2. Advanced quantum electrodynamics found the so-called anomalous magnetic moment to be 2.002... This was merely a correction on the basis laid down by Dirac.

$$\mathcal{H}_{SOC} = -\frac{e}{2m} \underline{S} \cdot \frac{1}{4\pi\epsilon_0} \frac{e}{mc^2 r^3} \underline{L} = \frac{e^2}{8\pi\epsilon_0} \frac{1}{m^2 c^2 r^3} \underline{S} \cdot \underline{L} \tag{A.6}$$

This is the result after a classical approach. We should apply two corrections: quantum electrodynamics adds a factor 2 on the gyromagnetic ratio. The constant accelerating of the electron adds a factor $\frac{1}{2}$ through Thomas precession. Ironically, these two wrongs do make a right, giving more credit to our classical approach than might be appropiate. The important takeaway is that the Hamiltonian depends on the interaction of the spin of the electron and the angular momentum of the electron.

A.3. Electron transport on mesoscopic scale

At the mesoscopic scale, both classical and quantum mechanics fail to deliver an accurate model for electron transport. Here, electrons maintain quantum coherence over the size of the conductor, but interact with it like particles. In other words, if the quantum waves of the electrons can be coherent with eachother whilst travelling through, and interacting with the conductor, we must find a formalism that contains both quantum as classical implications. Ohm's law does not account for wave-like behaviour, such as interference, discrete modes of the and boundary scattering.
The associated scattering problem is described in the Landauer-Büttiker formalism. Incoming electron waves interact in the mesoscopic region defined by the conductor. Some are transmitted into the other lead (or the Büttiker probe), others reflect back into the reservoir it came from. These reservoirs must be macroscopic, and in combination with NEGF, we treat the reservoirs (leads and büttiker probe) as semi-infinite, as seen in chapter 4. The scattering process is elastic by definition in the formalism. Ref [4] as mentioned in section 3.2.2 showed that symmetry of the conductor is safe to assume, so no impurities exist that can cause inelastic scattering in CISS experiments. The **scattering matrix** enables us to write this formalism down. It connects the amplitude of the incoming electron wave to the amplitude of the outgoing electron wave, describing transport. A thorough bottom up explanation can be found in reference [7].

[3]We need to account for special relativity in the Schrödinger equation to find spin, thus one can imagine that at such speeds, the proton seems almost like a full current loop

A.4. The transfer Hamiltonian

In the precious section we have discussed the SK Hamiltonian for a single atom. For transport, we also need couplings between orbitals centred on the neighbouring atoms. Summing over all, atoms, orbitals and sites, the Hamiltonian is described by:

$$\mathcal{H} = \sum_{\mu,\nu,i} h_{\mu\nu}^{(i)} + \sum_{\mu,\nu,i,j} h_{\mu\nu}^{(i,j)} \tag{A.7}$$

The effective Hamiltonian only includes nearest neighbour couplings and the first order perturbation theory implies no interactions beyond a certain regime. Geyer [9] showed that both second order spin-coupling and second order tight binding interactions (double electron hopping) are not of significant influence. We can describe all interactions between nearest neighbours, where we denote this with a transfer Hamiltonian:

$$\mathcal{H}_{\mu\nu}^{\langle ij\rangle} = n^{\parallel}(\mu, ij) \cdot n^{\parallel}(\nu, ji) V_{\mu\nu\sigma} + n^{\perp}(\mu, ij) \cdot n^{\perp}(\nu, ji) V_{\mu\nu\pi} \tag{A.8}$$

where μ en ν describe the interacting orbitals of neighbouring atoms i and j respectively. The vectors n describe the spatial orientation of the neighbours within the hexagonal structure. It is a function of our local coordinate system, which is a construct of axial and polar vectors:

$$\underline{n}(x, i) = (\cos\phi_i, \sin\phi_i, 0) \tag{A.9}$$

$$\underline{n}(y, i) = (-\sin\phi_i, \cos\phi_i, 0) \tag{A.10}$$

$$\underline{n}(z, i) = (0, 0, 1) \tag{A.11}$$

Each site has its own right-handed local coordinate system. The vectors are either parallel, $\underline{n}^{\parallel}$, or perpendicular, $\underline{n}^{\perp}$, to the global z-axis. We find different expressions for different orbitals, since the orbitals vary in their associated angular momentum. The 2p orbitals are described by:

$$\underline{n}^{\parallel}(\mu, ij) = \frac{\underline{R}_{ij} \cdot \underline{n}(\mu, i)\underline{R}_{ij}}{|\underline{R}_{ij}|^2} \tag{A.12}$$

$$\underline{n}^{\perp}(\mu, ij) = \underline{n}(\mu, i) - n^{\parallel}(\mu, ij) \tag{A.13}$$

And for the 2s orbital we find:[4]

$$\underline{n}^{\parallel}(\mu, ij) = \frac{\underline{R}_{ij}}{|\underline{R}_{ij}|^2} \tag{A.14}$$

$$\underline{n}^{\perp}(\mu, ij) = 0 \tag{A.15}$$

The newly introduced variables are $\underline{R}_{ij} = \underline{R}_j - \underline{R}_i$ and $\underline{n}(\mu, i)$, the unit vector following from equations A.9 through A.11 [18].

This construct is limited. The p_z-orbitals extend out the plain along which the carbon hexagons are oriented. In nanotubes, these orbitals extend outwards, in our construct, the orbitals are a bit twisted along the helical curl. Hence previous models do not fully reflect the p_z-p_z-orbital couplings in our case. p_z orbitals are of highest importance, as the energy of the electrons in this orbital are close to the Fermi energy.
The notation ensures that the Hamiltonian only includes nearest neighbour couplings, so a superposition of multiple $\underline{n}^{\perp}$ and $\underline{n}^{\parallel}$ is not allowed. Furthermore, we neglect the terms beyond second order in ξ_p and ξ_{sp}.

[4] The 1s orbital is completely surrounded by the 2s orbital and is therefore not relevant in the electron transport. The modelled Hamiltonian contains the eight orbitals associated with principal quantum number n=2. The 1s orbital is completely omitted.

A.5. Projection matrices

In this model, we use the z-axes as a base. This means that the $+z$-axis and $-z$-axis form the standard basis. To orient the Büttiker probe, we create the associated projection matrix through the outer product:

$$\begin{pmatrix}1\\0\end{pmatrix}\begin{pmatrix}1 & 0\end{pmatrix} = \begin{pmatrix}1 & 0\\0 & 0\end{pmatrix} \tag{A.16}$$

for the +z-axis and

$$\begin{pmatrix}0\\1\end{pmatrix}\begin{pmatrix}0 & 1\end{pmatrix} = \begin{pmatrix}0 & 0\\0 & 1\end{pmatrix} \tag{A.17}$$

for the -z-axis.
If we look at the magnetisation, this only creates a difference in transmission. We use the parameter p to describe the polarisation. The left lead will use p as value for the polarisation. This results in the following projection matrix:

$$\Gamma \propto \gamma\left[p\begin{pmatrix}1\\0\end{pmatrix}\begin{pmatrix}1 & 0\end{pmatrix} + (1-p)\begin{pmatrix}0\\1\end{pmatrix}\begin{pmatrix}0 & 1\end{pmatrix}\right] = \gamma\begin{pmatrix}p & 0\\0 & 1-p\end{pmatrix}. \tag{A.18}$$

The equation above introduces a Γ. This is the scattering rate, or the quantifier for the coupling between the lead and the molecule. γ is a scalar for the scattering rate independent from p. More on the mathematical theory of mesoscopic transport can be found in Chapter 4.
The right lead has a different polarisation. We call this polarisation q. Since the relation with Γ is identical for both leads, we find an identical matrix. Then we use that $q = 1 - p$, as the total spin must be conserved. This results in a similar matrix:

For the magnetisation along the x-axis, we use a different basis to span the same space. Similar to the Pauli spin matrices, the matrices associated with the +x and -x-axis are respectively:

$$\begin{pmatrix}1\\1\end{pmatrix}\begin{pmatrix}1 & 1\end{pmatrix} = \begin{pmatrix}1 & 1\\1 & 1\end{pmatrix} \tag{A.19}$$

and

$$\begin{pmatrix}1\\-1\end{pmatrix}\begin{pmatrix}1 & -1\end{pmatrix} = \begin{pmatrix}1 & -1\\-1 & 1\end{pmatrix}. \tag{A.20}$$

The method to find the projection matrices for the leads is completely analogues to the case of the z-axes. For the left lead, polarisation p, we find

$$\Gamma \propto \gamma\left[\frac{1}{2}p\begin{pmatrix}1\\1\end{pmatrix}\begin{pmatrix}1 & 1\end{pmatrix} + \frac{1}{2}(1-p)\begin{pmatrix}1\\-1\end{pmatrix}\begin{pmatrix}1 & -1\end{pmatrix}\right] = \frac{1}{2}\gamma\begin{pmatrix}1 & -1+2p\\-1+2p & 1\end{pmatrix} \tag{A.21}$$

and for the right lead, with $q = 1 - p$, we find

$$\Gamma \propto \frac{1}{2}\gamma\begin{pmatrix}1 & -1+2q\\-1+2q & 1\end{pmatrix} = \frac{1}{2}\gamma\begin{pmatrix}1 & -1+2(1-p)\\-1+2(1-p) & 1\end{pmatrix} = \frac{1}{2}\gamma\begin{pmatrix}1 & 1-2p\\1-2p & 1\end{pmatrix}. \tag{A.22}$$

We're a factor $\frac{1}{2}$ appears to normalise the base vectors.